Diabolical conical intersections

David R. Yarkony

Department of Chemistry, Johns Hopkins University, Baltimore, Maryland 21218

In the Born-Oppenheimer approximation for molecular dynamics as generalized by Born and Huang, nuclei move on multiple potential-energy surfaces corresponding to different electronic states. These surfaces may intersect at a point in the nuclear coordinates with the topology of a double cone. These conical intersections have important consequences for the dynamics. When an adiabatic electronic wave function is transported around a closed loop in nuclear coordinate space that encloses a conical intersection point, it acquires an additional geometric, or Berry, phase. The Schrödinger equation for nuclear motion must be modified accordingly. A conical intersection also permits efficient nonadiabatic transitions between potential-energy surfaces. Most examples of the geometric phase in molecular dynamics have been in situations in which a molecular point-group symmetry required the electronic degeneracy and the consequent conical intersection. Similarly, it has been commonly assumed that the conical intersections facilitating nonadiabatic transitions were largely symmetry driven. However, conical intersections also occur in the absence of any symmetry considerations. This review discusses computational tools for finding and characterizing the conical intersections in such systems. Because these purely accidental intersections are difficult to anticipate, they may occur more frequently than previously thought and in unexpected situations, making the geometric phase effect and the occurrence of efficient nonadiabatic transitions more commonplace phenomena. [S0034-6861(96)00404-7]

CONTENTS

I. INTRODUCTION

Within the Born-Oppenheimer approximation for molecular systems, the nuclei move on a single potential-energy surface created by the faster moving electrons. This approximation is extremely reliable for describing near-equilibrium properties of most molecules. However, for a reaction as simple as the exchange reaction $H_2+H\rightarrow H+H_2$ problems can arise. A recent series of resonance-enhanced multiphoton ionization and time-of-flight mass spectroscopic measurements characterized the product rotational-state distributions for the $D+H_2$ reactions (Kliner *et al.*, 1990, 1991; Adelman *et al.*, 1992)

$$D+H_2(v=0,j)\rightarrow HD(v'=0,j')+H, \tag{1.1a}$$

$$D+H_2(v=1,j)\rightarrow HD(v'=1,j')+H, \tag{1.1b}$$

where v is the vibrational quantum number. For reaction (1.1a) at a translation energy (E_{tr}) of 1.05 eV, "perfect" agreement (Wu and Kuppermann, 1993) between the theoretical predictions (Zhang and Miller, 1989; Blais *et al.*, 1990) and the experimental measurements (Kliner *et al.*, 1990) was obtained. However, for reaction (1.1b), that is, for $v=1$, agreement between theory (Zhang and Miller, 1989; Mielke *et al.*, 1992; Neuhauser *et al.*, 1992) and experiment (Kliner *et al.*, 1991) deteriorates, at virtually the same E_{tr}, E_{tr}=1.02 eV. The culprit is not, as might be expected, a problem with the potential-energy surface, the $1^2A'$ potential-energy surface, or the solution of the scattering problem. Rather, the culprit is a deficiency in the basic adiabatic Born-Oppenheimer nuclear Schrödinger equation. This deficiency is the result of conical intersections of the $1^2A'$

potential-energy surface with a second potential-energy surface of $^2A'$ symmetry,[1] the $2^2A'$ potential-energy surface (Wu and Kuppermann, 1993).

A point of conical intersection is a point in nuclear coordinate space at the confluence of two Born-Oppenheimer potential-energy surfaces. The local topology of the potential-energy surfaces at this point is that of a double cone, a diabolo (Berry and Wilkinson, 1984). Thus points of conical intersection are sometimes referred to, quite aptly we will argue, as diabolical points (Berry and Wilkinson, 1984). Conical intersections are to be distinguished from Renner-Teller or glancing intersections (Renner, 1934; Longuet-Higgins, 1961; Jungen and Merer, 1976). Three types of Renner-Teller intersections, labeled following Lee *et al.* (1984) and a Jahn-Teller intersection, a particular example of a conical intersection, are presented in Figs. 1(a)–1(c) and 1(d), respectively. A detailed discussion of the types of Renner-Teller intersections can be found in Lee *et al.* (1984). Jahn-Teller intersections are also well studied and have been the subject of many reviews (Englman, 1972; Bersuker 1984a, 1984b; Whetten *et al.*, 1985; Bersuker and Ogurtson, 1986). While it is not the purpose of this review to discuss Renner-Teller or Jahn-Teller intersections in detail, the differences between these two classes of surfaces of intersection have considerable relevance in the present context and are reviewed in Sec. II.

The effect of conical intersections on molecular processes may be classified as either direct or indirect, according to whether or not nuclear motion actually takes place on both surfaces in question. Direct effects are exhibited in radiationless decay of an excited state (Michl and Bonacic-Koutecky, 1990; Kato and Baba, 1995) and "nonadiabatic recrossing" (Kash *et al.*, 1994; Waschewsky *et al.*, 1994), in which nuclear motion occurs on two potential-energy surfaces although the overall process begins and ends on the same potential-energy surface, that is, it is ostensibly adiabatic. The more subtle indirect effect occurs in a true adiabatic, single potential-energy surface process, as a result of what is variously referred to as the geometric phase effect (Longuet-Higgins, 1961; Herzberg and Longuet-Higgins, 1963), molecular Aharonov-Bohm effect (Aharonov and Bohm, 1959; Mead and Truhlar, 1979; Mead, 1980a), or Berry phase effect (Berry, 1984). As a consequence of this effect, nuclear wave functions that are transported around a path that encloses a point of conical (as opposed to Renner-Teller) intersection acquire an additional nondynamical or geometric phase. This accumulated phase compensates for the changes in the phase of the adiabatic electronic wave function, which cannot be both real-valued and continuous. It is this indirect geometric phase effect that results in the disagreement between theory and experiment in the $H+H_2$ scattering noted above (Wu and Kuppermann, 1993).

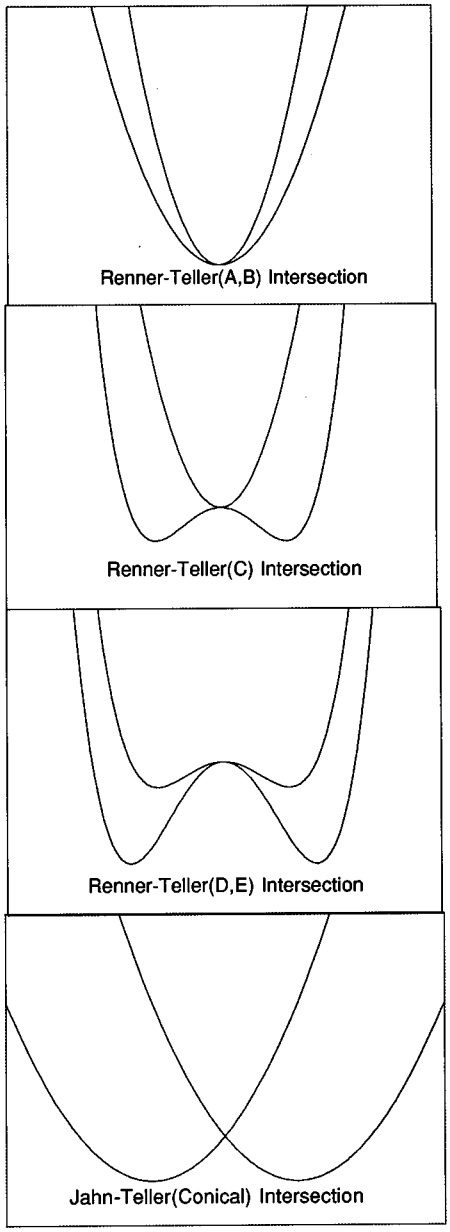

FIG. 1. Cross sections $C1$ and $C2$ of surfaces of revolution exhibiting Renner-Teller and Jahn-Teller intersections, after Longuet-Higgins (1961) and Lee *et al.*, (1984): (1) $C1=\alpha_1\rho^2$, $C2=\alpha_2\rho^2$; (2) $C1=-\alpha_1\rho^2+\beta_1\rho^4$, $C2=\alpha_2\rho^2$; (3) $C1=-\alpha_1\rho^2+\beta\rho^4$, $C2=-\alpha_2\rho^2+\beta_2\rho^4$; (d) $C1=-\alpha_1\rho+\beta\rho^2$, $C2=\alpha_1\rho+\beta_2\rho^2$.

The subtle aspect of the geometric phase effect is that it shows up when a closed loop around the conical intersection becomes energetically accessible, regardless of the energy of the conical intersection itself, so that the nuclei need never move on the second potential-energy surface for that surface to affect the dynamics. In the H_3 system the conical intersection is approximately 1.5 eV higher than the lowest-energy path, so that the effect of the conical intersection on the dynamics was not widely anticipated (Mead, 1980c).

While the importance of the energetically inaccessible

[1]The spectroscopic notation $^2A'$ refers to an electronic state that is a spin-doublet and whose spatial part carries the A' representation of the C_s group.

conical intersections in this low-energy scattering of H_2 by H came as something of a surprise Goss-Levi, 1993; Wu and Kuppermann, 1993)—despite its prediction more than a decade earlier (Mead, 1980c)—the role of conical intersections in other observable phenomena has long been recognized. This topological feature is well known to provide an efficient pathway, a funnel, for radiationless decay of optically prepared electronically excited states in both small molecular systems (Desouter-Lecomte *et al.*, 1979) and large (biologically relevant) ones (Bernardi, Olivucci, Ragazos, and Robb, 1992). Even the geometric phase effect has been known for over three decades in molecular spectroscopy where, in an explicitly two-state formulation, it produces the dynamic Jahn-Teller effect (Gerber and Schumacher, 1978; Morse *et al.*, 1983). This effect is well understood as a consequence of the pioneering work of Longuet-Higgins (Longuet-Higgins *et al.*, 1958; Longuet-Higgins, 1961).

Although initially ''discovered'' in the context of the Born-Oppenheimer electronic Hamiltonian, the geometric phase effect may be evinced in any parametrically dependent Hamiltonian. This was first appreciated by Berry (1984). Because of the enormous impact of Berry's work, the geometric phase effect is frequently referred to as the Berry phase effect. The implications of the geometric/Berry phase effect for general adiabatic processes have been reviewed in this journal (Mead, 1992) and elsewhere (Jackiw, 1988; Shapere and Wilczek, 1989; Zwanziger *et al.*, 1990; Bohm *et al.*, 1991).

The impact of the geometric phase effect on molecular dynamics reflects the prevalence of the requisite conical intersections. Traditionally conical intersections were viewed as comparatively rare topological features, invoked when molecular point-group symmetry required them, normal degeneracies (Tinkham, 1964), as in the Jahn-Teller effect, or permitted them, in a class of accidental degeneracies referred to as symmetry-allowed (Frey and Davidson, 1990). Intersections of two surfaces of the *same* symmetry, another class of accidental degeneracies, although in principal known to exist (von Neumann and Wigner, 1929), were largely ignored. In fact, the existence of conical intersections of two states with the same point-group symmetry had been a matter of some controversy. The conditions under which two potential-energy surfaces may intersect, referred to as the noncrossing rule, were first considered by von Neumann and Wigner (1929). In the 1970s several groups argued against the rule's validity (Naqvi, 1972; Hatton, 1976, 1977; Hatton *et al.*, 1976, 1977), although it is in fact quite valid (von Neumann and Wigner, 1929; Herzberg and Longuet-Higgins, 1963; George *et al.*, 1975; Longuet-Higgins, 1975; Stone, 1976; Mead, 1979); see Sec. II.

Conical intersections of two states of the same symmetry, a hitherto underappreciated class of conical intersections, are the focus of this review. The occurrence of this class of conical intersection and the concomitant geometric phase effect present a particularly diabolical situation, since neither the existence of the conical intersection nor the nuclear trajectories that can result in the geometric phase effect can be anticipated on the basis of group-theoretical arguments. However, the development of new computational tools (Lengsfield and Yarkony, 1992; Bearpark *et al.*, 1994; Yarkony, 1995) has made it possible to locate conical intersections in general molecular systems and to characterize readily the nuclear trajectories associated with the geometric phase (Yarkony, 1996a; 1996b) without the help of point-group symmetry. These techniques locate conical intersections directly, that is, without tedious determination of the potential-energy surfaces in question. Recent work (Bernardi, De, *et al.*, 1990; Bernardi, Olivucci, *et al.*, 1990; Bernardi, Olivucci, Ragazos, and Robb, 1992; Bernardi, Olivucci, Robb, and Tonachini, 1992; Manaa and Yarkony, 1994; Yarkony, 1994; Hettema and Yarkony, 1995) has suggested that conical intersections of two states of the same symmetry are much more common than previously anticipated. This will have important consequences for nuclear dynamics. In view of the important questions raised by this ongoing research, this review was undertaken to summarize the current state of this reemerging area.

Section II introduces the tools that will permit the computational studies. To place these algorithms in their proper perspective, the elementary theory of nonadiabatic processes, with particular emphasis on conical intersections and the geometric phase, is reviewed. Readers interested in a more detailed mathematical overview of the geometric phase and its impact in molecular dynamics should consult Mead's review in this journal (Mead, 1992). In Sec. III the numerical procedures are used to characterize conical intersections of two states of the same symmetry that induce either the geometric phase effect in an adiabatic process or an electronically nonadiabatic transition. Section IV summarizes and discusses the implications of the work reviewed herein.

II. CONCEPTS FOR NONADIABATIC PROCESSES

A. Basic principles

We begin by partitioning the total Hamiltonian $H^T(\mathbf{r},\mathbf{R})$ as follows:

$$H^T(\mathbf{r},\mathbf{R})=\sum_{\alpha=1}^{N^{\rm nuc}} \frac{-1}{2M_\alpha}\nabla_\alpha^2+H(\mathbf{r};\mathbf{R})\equiv T^{\rm nuc}+H(\mathbf{r};\mathbf{R}). \tag{2.1}$$

Here $\mathbf{r}$ and $\mathbf{R}$ denote the coordinates of the N^e electrons and $N^{\rm nuc}$ nuclei, respectively, in a space-fixed frame and $T^{\rm nuc}$ is the nuclear kinetic operator. The use of a space-fixed frame is adequate for the presentation that follows. The conversion to a coordinate system that separates internal degrees of freedom from translations and rotations is a nontrivial task. See, for example, Wu and Kuppermann (1993); Wu *et al.* (1994); Kendrick and Pack (1996a). In this work unless otherwise noted relativistic effects will be ignored, so that $H(\mathbf{r};\mathbf{R})$ is the nonrelativistic Born-Oppenheimer *electronic* Hamiltonian. With this approximation, the $2S+1$ sublevels of an electronic

state with total electron spin S can never mix. In this case only the scalar (Abelian), as opposed to the matrix or non-Abelian (Wilczek and Zee, 1984; Moody *et al.*, 1986) realization of the geometric phase effect can occur. The reader interested in the non-Abelian case should begin by consulting Mead (1992).

We define a set of *adiabatic* electronic wave functions, $\Psi_I(\mathbf{r};\mathbf{R})$, by

$$[H(\mathbf{r};\mathbf{R})-E_I(\mathbf{R})]\Psi_I(\mathbf{r};\mathbf{R})=0. \tag{2.2}$$

This set is in principle complete. As a consequence of the partitioning in Eq. (2.1), the electronic wave functions and the Hamiltonian depend only parametrically on $\mathbf{R}$, while the eigenvalues $E_I(\mathbf{R})$ depend explicitly on $\mathbf{R}$. A semicolon is used to distinguish this parametric dependence. $E_I(\mathbf{R})$ actually depends only on the $3N^{\rm nuc}-6\equiv N^{\rm int}$ subset of the nuclear coordinates referred to as the internal coordinates and denoted $\mathbf{R}^i$. However, it will be notationally convenient to suppress this distinction unless specifically required.

The $\Psi_I(\mathbf{r};\mathbf{R})$ are assumed to be expanded in a basis of N^e-electron functions, referred to as configuration-state functions (CSFs; Shavitt, 1976), and denoted $\Psi_\alpha(\mathbf{r};\mathbf{R})$, $\alpha=1-N^{\rm CSF}$. It will be assumed, if required, that $N^{\rm CSF}$ can be quite large, $>10^6$. These basis functions are symmetry adapted, that is, they are eigenfunctions of S^2, antisymmetric under electron interchange, and carry an irreducible representation of the spatial point group of the nuclei. The CSFs are linear combinations of Slater determinants, antisymmetrized products of molecular spin orbitals, $\xi_i(\mathbf{r};\mathbf{R})\gamma_i$, $i=1-N^{\rm mso}$ and $\gamma_i=\alpha$ or β, that is,

$$\psi_\alpha=\sum_i d_i^\alpha A\prod_{j=1}^{N^e}\xi_{i_j}\gamma_{i_j}, \tag{2.3}$$

where A is the N^e particle antisymmetrizer. The molecular orbitals $\xi_i(\mathbf{r};\mathbf{R})$ are obtained from a self-consistent-field procedure, which imparts the indicated $\mathbf{R}$ dependence (Lengsfield and Yarkony, 1992). Here and throughout this work the $\mathbf{r}$ and $\mathbf{R}$ dependence of a function may be suppressed for clarity when no confusion will result. Also adopted is the convention that vectors (matrices) are indicated by bold (bold/italic) typeface. Thus the real-valued electronic wave function is

$$\Psi_I(\mathbf{r};\mathbf{R})=\sum_{\alpha=1}^{N^{\rm CSF}} c_\alpha^I(\mathbf{R})\psi_\alpha(\mathbf{r};\mathbf{R})\equiv\mathbf{c}^I(\mathbf{R})^\dagger\boldsymbol{\psi}(\mathbf{r};\mathbf{R}). \tag{2.4a}$$

The $\mathbf{c}^I(\mathbf{R})$ satisfy the secular problem

$$[\boldsymbol{H}(\mathbf{R})-\boldsymbol{I}E_I(\mathbf{R})]\mathbf{c}^I(\mathbf{R})=\mathbf{0} \tag{2.5}$$

where $\boldsymbol{H}(\mathbf{R})$ is the electronic Hamiltonian matrix in the CSF basis.

At any particular nuclear configuration $\mathbf{R}$, it is possible to choose the adiabatic electronic wave functions to be real valued. However, since the electronic wave function is determined only up to a geometry-dependent phase factor, it may not be possible, as noted in the Introduction, to require the wave functions to be real valued at all nuclear configurations and still preserve continuity with respect to $\mathbf{R}$. This is a key issue in the theory of conical intersections and is the essential idea behind the geometric phase effect. To include the possibility of a geometry-dependent phase factor, we define, following Mead and Truhlar (1979), a gauge transformation

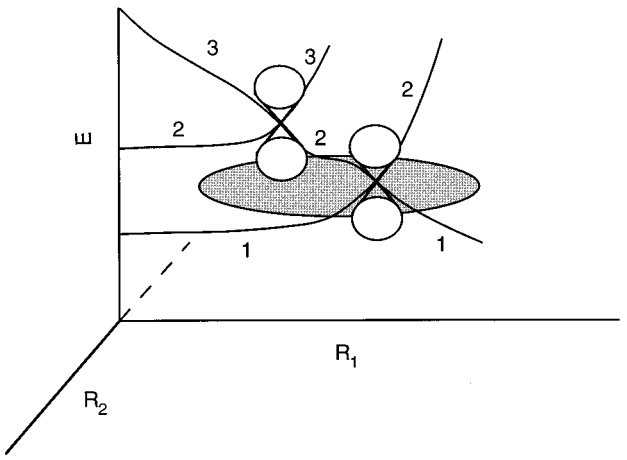

FIG. 2. Conical intersections of two-dimensional potential-energy surfaces for states (1,2) and (2,3) in a region of nuclear coordinate space indicated by the shaded oval.

$$\tilde{\Psi}_I(\mathbf{r};\mathbf{R})\equiv e^{iA_I(\mathbf{R})}\Psi_I(\mathbf{r};\mathbf{R}), \tag{2.4b}$$

where the $A_I(\mathbf{R})$ are chosen to make $\tilde{\Psi}_I(\mathbf{r};\mathbf{R})$ single-valued and the $\Psi_I(\mathbf{r};\mathbf{R})$ are the real-valued solutions to Eq. (2.2) or Eq. (2.5). Gauge transformations of this type have been used previously in multistate problems by Longuet-Higgins in his classic treatment of the dynamic Jahn-Teller effect noted above (see also Sec. II.D) and by Mead (1983) in his treatment of conical intersections in X_3 systems. The $\mathbf{R}$ dependence of $A_I(\mathbf{R})$ must reflect the presence of any conical intersection in accordance with the Berry phase condition given below. Thus the $A_I(\mathbf{R})$ can be constructed only after the conical intersections have been located. While a generally applicable approach for determining the $A_I(\mathbf{R})$ has been suggested (Kendrick and Mead, 1995), its determination remains a nontrivial task. Note that a distinct geometric phase factor $A_I(\mathbf{R})$ may be required for each state. This reflects the observation (see Fig. 2 and Sec. III.D) that conical intersections involving distinct, but nondisjoint, pairs of states are possible, even in a small region of nuclear coordinate space.

The total wave function, $\Psi_k^T(\mathbf{r},\mathbf{R})$, expanded as

$$\Psi_k^T(\mathbf{r},\mathbf{R})=\sum_{I=1}^{N^a}\chi_I^k(\mathbf{R})e^{iA_I(\mathbf{R})}\Psi_I(\mathbf{r};\mathbf{R})$$

$$\equiv\boldsymbol{\chi}^k(\mathbf{R})^\dagger\tilde{\boldsymbol{\Psi}}(\mathbf{r};\mathbf{R}), \tag{2.6}$$

satisfies the total, time-independent Schrödinger equation $(H^T-E)\Psi_k^T(\mathbf{r},\mathbf{R})=0$. The expansion of Ψ^T on the right-hand side of Eq. (2.6) represents the Born-Huang approximation (Born and Huang, 1954; Ballhausen and Hansen, 1972). The basic premise of this approach is

that the preliminary solution of Eq. (2.2) allows for the drastic truncation of the summation in Eq. (2.6), that is, N^a is small, 1, 2, or 3, usually. The strictly adiabatic limit, the Born-Oppenheimer approximation, corresponds to N^a=1. If N^a were to be large, little if anything would be gained by separating electronic and nuclear motion. In such a case the nuclei and electrons should be treated on an equal footing. Such completely nonadiabatic treatments have been performed to date only for small molecular systems (Deumens *et al.*, 1994), including the classic treatment of H_2 by Kolos and Wolniewicz (1963).

Using expansion (2.6) in the time-independent Schrödinger equation gives the nuclear Schrödinger equation for $\boldsymbol{\chi}^k(\mathbf{R})$:

$$\left[\sum_{\alpha=1}^{N^{\rm nuc}} \frac{-1}{2M_\alpha}\nabla_\alpha^2 + E_I(\mathbf{R}) - E_k\right]\chi_I^k(\mathbf{R}) = \sum_{J=1}^{N^a}\sum_{\alpha=1}^{N^{\rm nuc}}\left[\frac{1}{2M_\alpha}\{-\tilde{k}_\alpha^{IJ}(\mathbf{R}) + \nabla_\alpha\cdot\tilde{\mathbf{f}}_\alpha^{IJ}(\mathbf{R}) + \tilde{\mathbf{f}}_\alpha^{IJ}(\mathbf{R})\cdot\nabla_\alpha\}\right]\chi_J^k(\mathbf{R}), \tag{2.7a}$$

or using real-valued wave functions

$$\left[\sum_{\alpha=1}^{N^{\rm nuc}} \frac{+1}{2M_\alpha}(-i\nabla_\alpha + \mathbf{A}_I^\alpha)^2 + \bar{E}_I(\mathbf{R}) - E_k\right]\chi_I^k(\mathbf{R})$$
$$= \sum_{J(\neq I)}^{N^a} e^{iA_{JI}(\mathbf{R})}\sum_{\alpha=1}^{N^{\rm nuc}}\left[\frac{1}{2M_\alpha}\{-k_\alpha^{IJ}(\mathbf{R}) + i(-i\nabla_\alpha + \mathbf{A}_J^\alpha)\cdot\mathbf{f}_\alpha^{IJ}(\mathbf{R}) + i\mathbf{f}_\alpha^{IJ}(\mathbf{R})\cdot(-i\nabla_\alpha + \mathbf{A}_J^\alpha)\}\right]\chi_J^k(\mathbf{R}), \tag{2.7b}$$

where the derivative operator acts on all quantities to its right, $\boldsymbol{A}_J^\alpha(\mathbf{R})=\nabla_\alpha A_J(\mathbf{R})$, $A_{JI}(\mathbf{R})=A_J(\mathbf{R})-A_I(\mathbf{R})$. The first derivative couplings or simply the derivative couplings, $\tilde{\mathbf{f}}_\alpha^{JI}(\mathbf{R})$, are given by

$$\tilde{\mathbf{f}}_\alpha^{JI}(\mathbf{R}) = \langle\tilde{\Psi}_J(\mathbf{r};\mathbf{R})|\nabla_\alpha\tilde{\Psi}_I(\mathbf{r};\mathbf{R})\rangle_{\mathbf{r}}, \tag{2.8}$$

$$\tilde{k}_\alpha^{JI}(\mathbf{R}) = \langle\nabla_\alpha\tilde{\Psi}_J(\mathbf{r};\mathbf{R})\cdot|\nabla_\alpha\tilde{\Psi}_I(\mathbf{r};\mathbf{R})\rangle_{\mathbf{r}} \tag{2.9a}$$

$$= \sum_{K=1}^{N^{\rm CSF}}\tilde{\mathbf{f}}_\alpha^{KJ}(\mathbf{R})^*\cdot\tilde{\mathbf{f}}_\alpha^{KI}(\mathbf{R}), \tag{2.9b}$$

and finally

$$\bar{E}_I(\mathbf{R}) = E_I(\mathbf{R}) + \sum_{\alpha=1}^{N^{\rm nuc}}\frac{k_\alpha^{II}}{2M_\alpha}. \tag{2.10}$$

Here the superscript ˜ on a quantity will be used to denote the use of complex-valued electronic wave functions and will be omitted when real-valued wave functions are used. The subscript(s) on $\langle\cdots|\cdots\rangle$ will denote the coordinates being integrated and will be suppressed when no confusion will arise. In deriving Eq. (2.7) we have used the relation

$$\nabla_\alpha f_\alpha^{JI}(\mathbf{R}) = \langle\Psi_J(\mathbf{r};\mathbf{R})|\nabla_\alpha^2\Psi_I(\mathbf{r};\mathbf{R})\rangle_{\mathbf{r}} + k_\alpha^{JI}(\mathbf{R}). \tag{2.11}$$

The equivalence of Eqs. (2.7a) and (2.7b) is readily established by inserting Eq. (2.4b) into Eqs. (2.8) and (2.9a) and inserting the result into Eq. (2.7a).

The Berry phase condition (Berry, 1984) is a statement about the line integral of $\tilde{\mathbf{f}}_\alpha^{II}(\mathbf{R})$ around a closed loop C. Note that $\tilde{\mathbf{f}}_\alpha^{II}(\mathbf{R})=i\boldsymbol{A}_I^\alpha(\mathbf{R})\neq 0$ whereas $\mathbf{f}_\alpha^{II}(\mathbf{R})=0$. For $N^{\rm int}$=3 the accumulated phase around the closed loop C is given by

$$\gamma_I(C) \equiv i\oint_C\tilde{\mathbf{f}}^{II}(\mathbf{R}^i)\cdot d\mathbf{R}^i = -\oint_C\nabla A_I(\mathbf{R}^i)\cdot d\mathbf{R}^i \tag{2.12a}$$

$$= -\,\mathrm{Im}\int\int_C(\nabla\times\tilde{\mathbf{f}}^{II})\cdot d\mathbf{S}. \tag{2.12b}$$

Berry used Eq. (2.12b) to show that $\gamma_I(C) = \pm\pi(e^{i\gamma_I(C)}=-1)$ if C encompasses a conical intersection and zero ($e^{i\gamma_I(C)}=1$) otherwise, so that the associated wave function changes sign when a closed loop enclosing a conical intersection is traversed (Berry, 1984). The equivalences between Eqs. (2.12a) and (2.12b) rely on Stokes' theorem and must be generalized when $N^{\rm int}$>3 (Berry, 1984). Note that $\tilde{\mathbf{f}}^{II}$ is not the gradient of a scalar, whereas ∇A_I clearly is. Thus, from Eq. (2.12a) and Stokes' theorem, ∇A_I must be singular at the conical intersection. This has implications for the numerical procedures that employ the $\mathbf{A}_J^\alpha(\mathbf{R})$ (Kendrick and Pack, 1996a,1996b).

From Eq. (2.7b) it can be seen that the effect of conical intersections is to introduce the $\mathbf{A}_J^\alpha(\mathbf{R})$ into the nuclear Schrödinger equation. The $\mathbf{A}_J^\alpha(\mathbf{R})$ play the role of vector potentials analogous to those that appear in electromagnetic theory (Schiff, 1960). Since the $\mathbf{A}_J^\alpha(\mathbf{R})$ are singular at a conical intersection, the "magnetic field" corresponding to these vector potentials, $\nabla\times(\nabla A_I)$, is zero everywhere except at the conical intersection where it has a delta-function singularity. (Mead and Truhlar, 1979). Previously Aharonov and

Bohm (1959) had considered the effect of a true magnetic field confined to a narrow solenoid. It was for this reason that Mead (1980a) suggested the name Molecular Aharonov-Bohm effect for what is now referred to as the geometric or Berry phase effect.

If the adiabatic basis is complete (not the operative assumption in this work), Eq. (2.7a) can be written, with the help of Eq. (2.9a), in gauge-covariant form as (Moody *et al.*, 1986; Bohm, Kendrick, and Loewe, 1992; Bohm, Kendrick, Loewe, and Boya, 1992)

$$\sum_{J=1}^{N^a}\left[\sum_{K=1}^{N^a}\sum_{\alpha=1}^{N^{\rm nuc}}\frac{-1}{2M_\alpha}(\nabla_\alpha\delta_{IK}+\mathbf{f}_\alpha^{IK})\cdot(\nabla_\alpha\delta_{KJ}+\mathbf{f}_\alpha^{KJ})+E_I(\mathbf{R})\,\delta_{IJ}\right]\boldsymbol{\chi}_J^k(\mathbf{R})=E_k\boldsymbol{\chi}_I^k(\mathbf{R}). \tag{2.7a'}$$

These analogies have been used to invoke gauge-theory techniques into the treatment of conical intersections. (Zygelman 1987; Jackiw 1988; Pacher *et al.*, 1989).

It may appear at this point that the existence of a conical intersection completely invalidates the standard Born-Huang equations, that is Eq. (2.7b) without the $\boldsymbol{A}_I^\alpha$. This is not the case. If the terms in Eq. (2.6) are reassociated as $[\chi_I^K(\mathbf{R})e^{iA_I(\mathbf{R})}]\Psi_I(\mathbf{r};\mathbf{R})\equiv\tilde{\chi}_I^K(\mathbf{R})\Psi_I(\mathbf{r};\mathbf{R})$, then the electronic wave functions remain real but double-valued functions. In this case no gauge or vector potentials appear in Eq. (2.7b). This is compensated for by the fact that the $\tilde{\chi}_I^K(\mathbf{R})$ are now also doubled valued. This approach was used by Longuet-Higgins in his treatment of the dynamic Jahn-Teller effect (Longuet-Higgins, 1961) and in recent treatments of H_3 and its isotopomers. (Wu and Kuppermann, 1993). It is, however, difficult to implement in general situations and computationally cumbersome, so that the use of vector potentials is preferred (Kendrick and Pack, 1996a).

The $\mathbf{f}_\alpha^{IJ}(\mathbf{R})$ are key to understanding the limitations of the single-state Born-Oppenheimer approximation. In the past they have been difficult to evaluate for wave functions of the form in Eq. (2.4a) when $N^{\rm CSF}$ is large. However, within the last decade computational techniques have been introduced that make the determination of the $\mathbf{f}_\alpha^{IJ}(\mathbf{R})$ tractable (Lengsfield and Yarkony, 1992).

The adiabatic correction, the term involving $k_\alpha^{II}(\mathbf{R})$ in Eq. (2.10), modifies the potential-energy surface $E_I(\mathbf{R})$. In general it represents a small mass-dependent and $\mathbf{R}$-dependent correction and is routinely neglected. However, as a conical intersection is approached, $k_\alpha^{II}(\mathbf{R})$ approaches positive infinity [though $\bar{E}_I(\mathbf{R})-\bar{E}_J(\mathbf{R})$ still becomes quite small] and thus cannot be ignored. See Sec. II.D for an example. This follows from Eq. (2.9b) and the fact that at a conical intersection the components of $\mathbf{f}^{IJ}(\mathbf{R})$ are infinite. (Lengsfield and Yarkony, 1992). As a result there is a node in $\boldsymbol{\chi}(\mathbf{R})$ at a conical intersection point. The adiabatic correction has been evaluated using specialized (Bishop and Cheung, 1983, 1984) and more conventional (Jensen and Yarkony, 1988) electronic structure techniques for small molecular systems, including H_2, BeH^+ (Bishop and Cheung, 1984) and LiH (Bishop and Cheung, 1983; Jensen and Yarkony, 1988). The correction has also been measured experimentally (Chen *et al.*, 1986).

In the adiabatic approximation the nuclear Schrödinger equation becomes

$$\left[\sum_{\alpha=1}^{N^{\rm nuc}}\frac{-1}{2M_\alpha}(\nabla_\alpha^2-\tilde{k}_a^{II}(\mathbf{R})-\nabla_\alpha\cdot\tilde{\mathbf{f}}_\alpha^{II}(\mathbf{R})-\tilde{\mathbf{f}}_\alpha^{II}(\mathbf{R})\cdot\nabla_\alpha)+E_I(\mathbf{R})-E_k\right]\chi_I^k(\mathbf{R})=0 \tag{2.13a}$$

or, using real-valued electronic wave functions,

$$\left[\sum_{\alpha=1}^{N^{\rm nuc}}\frac{-1}{2M_\alpha}(\nabla_\alpha^2-A_I^{\alpha^2}+k_\alpha^{II}-i\nabla_\alpha\cdot\mathbf{A}_I^\alpha-i\mathbf{A}_I^\alpha\cdot\nabla_\alpha)+E_I(\mathbf{R})-E\right]\chi_I^k(\mathbf{R})=0 \tag{2.13a'}$$

or, equivalently,

$$\left[\sum_{\alpha=1}^{N^{\rm nuc}}\frac{+1}{2M_\alpha}(-i\nabla_\alpha+\mathbf{A}_I^\alpha)^2+\bar{E}_I(\mathbf{R})-E\right]\chi_I^k(\mathbf{R})=0. \tag{2.13a''}$$

In the absence of a conical intersection, the phase gradients do not appear in Eq. (2.13a″), resulting in the standard adiabatic nuclear Schrödinger equation,

$$\left[\sum_{\alpha=1}^{N^{\rm nuc}}\frac{-1}{2M_\alpha}\nabla_\alpha^2+\bar{E}_I(\mathbf{R})-E\right]\chi_I^k(\mathbf{R})=0. \tag{2.13b}$$

The difference between Eqs. (2.13a″) and (2.13b) demonstrates the diabolical nature of conical intersections noted in the Introduction. The $\mathbf{A}_I^\alpha$ are required by an intersection of two potential-energy surfaces, only one of which explicitly appears in the formulation of the problem. If the existence of the conical intersection cannot be anticipated (or ruled out), the dynamical treatment may be flawed. The omission of the $\mathbf{A}_I^\alpha$ represents the problem with the $H+H_2$ dynamics noted in the Introduction. This point is illustrated further in Sec. II.D, which juxtaposes the Renner-Teller and Jahn-Teller problems.

In a sense the geometric phase effect is the price exacted for using an electronically adiabatic basis. An alternative approach, which seeks to retain compactness

in the Born-Huang expansion while avoiding the pitfalls of the adiabatic basis—such as the Berry phase effect and the numerical difficulties associated with the derivative couplings (Sidis, 1992)—uses *diabatic* electronic states (Smith, 1969) $\Psi_I^d(\mathbf{r};\mathbf{R})$ in expansion (2.6). To maintain the compactness of the expansion while eliminating the derivative couplings, diabatic electronic states should be constructed as a unitary transformation of the adiabatic states, using the criterion (Smith, 1969)

$$\left\langle \Psi_I^d(\mathbf{r};\mathbf{R}) \left| \frac{\partial}{\partial R_\alpha^{\rm int}} \Psi_J^d(\mathbf{r};\mathbf{R}) \right\rangle_{\mathbf{r}} = 0 \right.$$

for $\alpha=1-N^{\rm int}$. It is well known that the resulting system of partial differential equations is not solvable when $N^a<N^{\rm CSF}$ (McLachlan, 1961; Baer, 1975; Mead and Truhlar, 1982). However, approximate, or quasidiabatic states can be used (McLachlan, 1961; Werner *et al.*, 1988; Pacher *et al.*, 1989; Baer, 1992; Sidis, 1992; Ruedenberg and Atchity, 1993). We note for completeness that the development of adiabatic states can be rephrased in the language of gauge theory (Pacher *et al.*, 1989; Bohm, Kendrick, and Loewe, 1992; Bohm, Kendrick, Loewe, and Boya, 1992), with the transformation to diabatic states described as a $U(N)$ gauge transformation—a non Abelian gauge transformation such that in the new basis the $\bar{\mathbf{f}}^{IJ}=0$, where the overbar indicates that the new basis is used to evaluate the derivative couplings.

Diabatic states should be used only when N^a is required to be greater than 1, that is, if the nuclear dynamics involves more than one potential-energy surface. Thus, if single-surface nuclear dynamics can be assumed, one must be careful to watch out for possible geometry phase effects.

As noted previously, the effect of a conical intersection can be quite diabolical, since it need not be energetically accessible for its influence to be exerted. Thus it is desirable, if not essential, to be able to locate conical intersections of potential-energy surfaces and characterize the circumscribing paths directly, that is, without prior determination of the potential-energy surfaces themselves. Before describing algorithms to accomplish this, it is necessary to say something about the dimensionality of the surface of intersection. This information is contained in the noncrossing rule, to which we now turn.

B. Surfaces of intersection: Noncrossing rule

The noncrossing rule defines the conditions for which there will be degenerate roots in the electronic Schrödinger equation in the full infinite-dimensional Hilbert space, that is, degeneracies in Eq. (2.2) rather than Eq. (2.5). However, for anything but the simplest problems, Eq. (2.2) is necessarily approximated by a problem in a finite-dimensional space such as Eq. (2.5) (Yarkony, 1996a). The specific results for the full infinite-dimensional space differ from its finite-dimensional approximation. It is known, for example, that the rigorous symmetry-allowed intersections in the one-electron system H_2^+ become avoided intersections when basis-set methods are used (Hatton, 1976; Hatton *et al.*, 1976; Hatton, 1977; Hatton *et al.*, 1977). Still a careful statement of the noncrossing rule is possible and has been given in the nonrelativistic matrix case by Longuet-Higgins (1975) and in more general situations by Mead (1979). According to the noncrossing rule (paraphrasing Longuet-Higgins), for molecules with an even number of electrons or if electron spin is ignored, crossings are exceptional for two electronic states of the same symmetry in diatomic molecules but not in polyatomic molecules (Longuet-Higgins, 1975). This is a consequence of two conditions needing to be fulfilled (Longuet-Higgins, 1975). The solution of the two equations is possible in a molecule with two or more degrees of freedom, that is, a polyatomic molecule, but in general extremely unlikely in a diatomic molecule, which possesses only one internal degree of freedom.

For the subsequent analysis, we need to know the local topology of the surface of conical intersections. This result will be used in the computational characterization of the surface of intersection, as well as in computation of the closed paths surrounding the point of a conical intersection, which may exhibit the geometric phase effect. A perturbative approach will be used to develop this result. This perturbative approach was used previously by the present author to develop/justify an algorithm for the determination of conical intersections (Yarkony, 1994, 1995, 1996c) and by Mead in his seminal discussions of the geometric phase effect (Mead and Truhlar, 1979, 1983; Mead, 1980a, 1983, 1992; Thompson and Mead, 1985; Thompson *et al.*, 1985, Pacher *et al.*, 1989; Kendrick and Mead, 1995). The same perturbative approach was also applied by Mead to the noncrossing rule (Mead, 1979) and the behavior of derivative couplings in the vicinity of a conical intersection (Mead, 1983).

Assume that $\mathbf{R}_x$ is a point in nuclear coordinate space corresponding to an intersection of M potential-energy surfaces. A new basis for the electronic Hamiltonian is to be constructed from a fixed, geometry-independent transformation of the CSF basis. The first M components of this transformation are the $\mathbf{c}^I(\mathbf{R}_x)$, $I=1-M$ satisfying Eq. (2.5). We denote this as the Q space. Its orthogonal complement is the P space. The functions in the P space, denoted $\mathbf{C}^J(\mathbf{R}_x)^\dagger\boldsymbol{\psi}(\mathbf{r};\mathbf{R})$, $J=(M+1)-N^{\rm CSF}$, need only be orthogonal to, and noninteracting with, $\mathbf{c}^I(\mathbf{R}_x)^\dagger\boldsymbol{\psi}(\mathbf{r};\mathbf{R})$, $I=1-M$. The $\mathbf{C}^J(\mathbf{R}_x)$ are not in general eigenfunctions of $\boldsymbol{H}(\mathbf{R}_x)$. This basis has only a limited geometry dependence through the CSFs. It is similar to the "crude adiabatic" basis introduced by Longuet-Higgins in his treatment of the Jahn-Teller and Renner-Teller effects (Longuet-Higgins, 1961) and will be denoted as such subsequently.

In the crude adiabatic basis, at any $\mathbf{R}$ Eq. (2.5) becomes

$$\begin{pmatrix} \boldsymbol{H}^{QQ}(\mathbf{R})-\boldsymbol{I}E_I(\mathbf{R}) & \boldsymbol{H}^{QP}(\mathbf{R}) \\ \boldsymbol{H}^{PQ}(\mathbf{R}) & \boldsymbol{H}^{PP}(\mathbf{R})-\boldsymbol{I}E_I(\mathbf{R}) \end{pmatrix} \begin{pmatrix} {}^Q\mathbf{c}(\mathbf{R}) \\ {}^P\mathbf{C}(\mathbf{R}) \end{pmatrix} = \begin{pmatrix} \mathbf{0} \\ \mathbf{0} \end{pmatrix} \tag{2.14}$$

where

$$H_{IJ}^{QQ}(\mathbf{R})=\mathbf{c}^I(\mathbf{R}_x)^\dagger \boldsymbol{H}(\mathbf{R})\mathbf{c}^J(\mathbf{R}_x),$$

$$H_{IK}^{QP}(\mathbf{R})=\mathbf{C}^K(\mathbf{R}_x)^\dagger \boldsymbol{H}(\mathbf{R})\mathbf{c}^I(\mathbf{R}_x),$$

and

$$H_{KL}^{PP}(\mathbf{R})=\mathbf{C}^K(\mathbf{R}_x)^\dagger \boldsymbol{H}(\mathbf{R})\mathbf{C}^L(\mathbf{R}_x)$$

for $I,J\leqslant M$ and $K,L>M$. At $\mathbf{R}_x$, $H_{IK}^{QP}(\mathbf{R}_x)=0$, $H_{IJ}^{QQ}(\mathbf{R}_x)=0$, $I\neq J, H_{II}^{QQ}(\mathbf{R}_x)=E_I(\mathbf{R}_x)$ with $E_I(\mathbf{R}_x)-E_M(\mathbf{R}_x)\equiv\Delta E_{IM}(\mathbf{R}_x)=0$, $I=1-(M-1)$.

We wish to consider under what conditions there can be a crossing at a neighboring nuclear configuration $\mathbf{R}_\varepsilon$. At $\mathbf{R}_\varepsilon$ the Hamiltonian matrix in the CSF basis becomes $\boldsymbol{H}(\mathbf{R}_\varepsilon)=\boldsymbol{H}(\mathbf{R}_x)+\Sigma_{R_\alpha}[\partial\boldsymbol{H}(\mathbf{R}_r)/\partial R_\alpha]\delta R_\alpha$ at first order, where $\delta\mathbf{R}=\mathbf{R}_\epsilon-\mathbf{R}_x$. Here and below, derivatives taken with respect to R^i_α, denoted R_α for simplicity, will be indexed by the subscript α. Note that the changes in $\boldsymbol{H}(\mathbf{R})$ result from changes in both the Hamiltonian operator, through the electron-nuclei attraction term, and in the molecular orbitals $\boldsymbol{\xi}(\mathbf{r};\mathbf{R})$ used to construct the CSFs. Thus in the crude adiabatic basis

$$H_{II}^{QQ}(\mathbf{R}_\varepsilon)=E_I(\mathbf{R}_x)+\mathbf{g}^I(\mathbf{R}_x)^\dagger\cdot\delta\mathbf{R}, \tag{2.15a}$$

$$H_{IJ}^{QQ}(R_\varepsilon)=\mathbf{h}^{IJ}(\mathbf{R}_x)^\dagger\cdot\delta\mathbf{R}, \tag{2.15b}$$

where

$$g^I_\alpha(\mathbf{R}_x)=\mathbf{c}^I(\mathbf{R}_x)^\dagger[\partial\mathbf{H}(\mathbf{R}_x)/\partial R_\alpha]\mathbf{c}^I(\mathbf{R}_x)$$
$$=[\partial E_I(\mathbf{R}_x)/\partial R_\alpha],$$

and

$$h^{IJ}_\alpha(\mathbf{R}_x)=\mathbf{c}^I=(\mathbf{R}_x)^\dagger[\partial\boldsymbol{H}(\mathbf{R}_x)/\partial R_\alpha]\mathbf{c}^J(\mathbf{R}_x).$$

Since contributions from the P space alter the energy at second order [$H_{IK}^{QP}(\mathbf{R}_x)=0$; Mead, 1983] the degeneracy can only be preserved through first order provided certain conditions are satisfied. From the diagonal matrix elements we get $(M-1)$ conditions

$$\mathbf{g}^{IM}(\mathbf{R}_x)^\dagger\cdot\delta\mathbf{R}=0,\quad I<M, \tag{2.16a}$$

where $g^{IM}(\mathbf{R})\equiv g^I(\mathbf{R})-g^M(\mathbf{R})$, and from the off-diagonal matrix elements we get $M(M-1)/2$ conditions (Mead, 1979; Katriel and Davidson, 1980)

$$\mathbf{h}^{IJ}(\mathbf{R}_0)^\dagger\cdot\delta\mathbf{R}=0,\quad I<J\leqslant M. \tag{2.16b}$$

Equations (2.16a) and (2.16b) represent limitations on the displacements $\delta\mathbf{R}$. They provide the requisite statement concerning the local topology of the surface of conical intersection. The degeneracy will be lifted at first order, that is linearly in the displacements, provided $\delta\mathbf{R}$ is restricted to the space of dimension $\bar{M}=(M-1)(M+2)/2$ spanned by the vectors $\mathbf{g}^{IM}(\mathbf{R}_x)$, $I=1-(M-1)$, and $\mathbf{h}^{IJ}(\mathbf{R}_x)$, $I<J\leqslant M$. For $M=2$, the case of interest in this review, $\bar{M}=M$ and the above space will be referred to as the *g-h plane*. As explained more fully in Sec. II.D, the behavior of the phase of an electronic wave function transported along a *g-h path*, a closed loop in the *g-h* plane that encloses a conical intersection point, reflects the geometric phase effect.

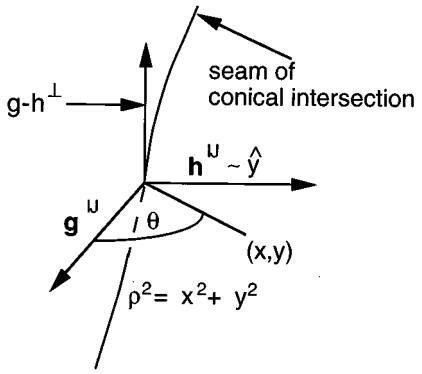

FIG. 3. *g-h* plane, *g-h*$^\perp$ vector and polar coordinates (ρ,θ) for a point (x,y) in the *g-h* plane. For pictorial simplicity $\mathbf{g}^{IJ}$ and $\mathbf{h}^{IJ}$ are taken to be perpendicular when defining (x,y).

The degeneracy is preserved through first order provided $\delta\mathbf{R}$ is restricted to the *g-h*$^\perp$ space, the space of dimension $N^{\text{int}}-\bar{M}$ orthogonal to the *g-h* plane. The *g-h* plane and *g-h*$^\perp$ space are illustrated in Fig. 3 for $N^{\text{int}}=3$. In this case the surface of intersection has dimension 1 and is referred to as a seam. The *g-h*$^\perp$ space is spanned by a single vector, which represents the tangent to the seam of conical intersection at $\mathbf{R}_x$.

Note that this result is a local one. For example, for $N^{\text{int}}=3$, more than one seam may exist; for $N^{\text{int}}=2$, more than one *isolated* point of conical intersection may exist. Examples of these situations are well known. The standard quadratic Jahn-Teller model (Longuet-Higgins, 1961; Meiswinkel and Köppel, 1990), a two-dimensional model, has four isolated points of conical intersection (Zwanziger and Grant, 1987). Additional examples will be indicated as the discussion proceeds.

The surface of intersection has (for $M=2$) dimension $N^{\text{int}}-2$ provided neither $\mathbf{g}^{IJ}(\mathbf{R})$ nor $\mathbf{h}^{IJ}(\mathbf{R})$ is identically zero. $\mathbf{g}^{IJ}(\mathbf{R})$ will not in general vanish identically. However, $\mathbf{h}^{IJ}(\mathbf{R})$ will vanish identically when $\mathbf{c}^I$ and $\mathbf{c}^J$ correspond to states of different symmetry. For states of the same spin-multiplicity but distinct point-group symmetry, the surface of intersection has dimension $\bar{N}^{\text{int}}-1$, where $\bar{N}^{\text{int}}$ is the number of totally symmetric internal degrees of freedom for the point group in question. For this case the intersection generally remains conical, with $\mathbf{h}^{IJ}$ contained in the space orthogonal to the totally symmetric internal degrees of freedom. An exception to this statement occurs for an intersection of an A' state and an A'' state in triatomic systems. In this case, the three internal coordinates transform as the totally symmetric, irreducible representation, so that there can be no coupling through first order in the crude adiabatic basis. In the true adiabatic basis, these states are not coupled by internal motions at all, but rather by overall molecular rotation. An example of this situation is, as discussed in II.D, a Renner-Teller intersection.

For the nonrelativistic electronic Hamiltonian consid-

ered here and $M=2$, the surface of intersection of states of different spin multiplicity [$\mathbf{h}^{IJ}(\mathbf{R})=0$ for all $\mathbf{R}$] will have dimension $N^{\rm int}-1$. However, this intersection is not conical, since for the nonrelativistic Hamiltonian no mixing of states of distinct spin multiplicity is possible. In the presence of the spin-orbit interaction, the character of this intersection changes. Even the dimensionality of the surface of intersection changes for odd-electron systems. The essential point is the role of Kramer's degeneracy (Tinkham, 1964; Truhlar *et al.*, 1975). The details of this issue are beyond the scope of the present review; they are discussed by Mead (1979).

C. Surfaces of intersection: Location

Two algorithms that directly locate points on the surface of conical intersections will be presented below, one based on the above perturbation theory and applicable to general polyatomic systems (Yarkony, 1995) and a second that finds its principle applications in triatomic systems (Manaa and Yarkony, 1990; Yarkony, 1990).

1. Conical intersections in general polyatomic systems

For general polyatomic systems $N^{\rm int}$ can be quite large, so that it may not be feasible or even desirable to characterize the entire surface of a conical intersection. The conical intersections that will be of most interest are those with energies accessible in chemical processes. Thus an algorithm is sought in which the energy of the point on the surface of a conical intersection is minimized. In addition it is frequently desirable, as in the photodissociation processes discussed in Sec. III, to restrict the range of nuclear configurations to be considered. Thus the problem at hand can be phrased as an energy minimization, subject to two classes of constraints: (i) the constraint of a conical intersection and (ii) the constraints on the nuclear configurations expressed as geometrical equality constraints, $K_i(\mathbf{R})$, $i=1-N^{\rm con}$. This constrained minimization will be accomplished using Lagrange multiplier techniques (Goldstein, 1950).

We begin by considering the imposition of the conical intersection constraint. Assume that $\mathbf{R}_0$ is a point in nuclear coordinate space near, but not at, an intersection of two potential-energy surfaces. Quasidegenerate perturbation theory will be used to determine a new geometry, $\mathbf{R}_x=\mathbf{R}_0+\delta\mathbf{R}$, which represents a point on the surface of conical intersection. As above, we use $\mathbf{c}^I(\mathbf{R}_0)$, $\mathbf{c}^J(\mathbf{R}_0)$ satisfying Eq. (2.5) at $\mathbf{R}_0$ to define the Q and P spaces. Note that I, $J(=I+1)$ need not be 1, 2. However, it is then necessary to include in the P space $\mathbf{c}^K(\mathbf{R}_0)$, $K=1-(I-1)$. At $\mathbf{R}_0$, $H_{KI}^{PQ}(\mathbf{R}_0)=0$, $H_{IJ}^{QQ}(\mathbf{R}_0)=0$, $H_{II}^{QQ}(\mathbf{R}_0)=E_I(\mathbf{R}_0)$, but $E_I(\mathbf{R}_0)\neq E_J(\mathbf{R}_0)$. We desire that, at $\mathbf{R}_x$, $E_I(\mathbf{R}_x)=E_J(\mathbf{R}_x)$ to first order. Since, as above, the P-space contributions change the energy at second order, $\delta\mathbf{R}$ must be chosen such that $\boldsymbol{H}^{QQ}(\mathbf{R}_x)$ has degenerate roots, that is,

$$\begin{aligned}\Delta H_{IJ}^{QQ}(\mathbf{R}_x)&\equiv H_{II}^{QQ}(\mathbf{R}_x)-H_{JJ}^{QQ}(\mathbf{R}_x)\\&=\Delta E_{IJ}(\mathbf{R}_0)+\mathbf{g}^{IJ}(\mathbf{R}_0)^{\dagger}\cdot\delta\mathbf{R}\\&=0\end{aligned}\tag{2.17a}$$

and

$$H_{IJ}^{QQ}(\mathbf{R}_x)=\mathbf{h}^{IJ}(\mathbf{R}_0)^{\dagger}\cdot\delta\mathbf{R}=0.\tag{2.17b}$$

Note that $\Delta H_{IJ}^{QQ}(\mathbf{R}_0)=\Delta E_{IJ}(\mathbf{R}_0)$ and $(\partial/\partial R_\alpha)\Delta H_{II}^{QQ}(\mathbf{R}_0)=g_\alpha^{IJ}(\mathbf{R}_0)$. Equations (2.17a) and (2.17b), represent the desired constraints.

On the basis of the above discussion, the following Lagrangian is to be minimized:

$$\begin{aligned}L(\mathbf{R},\boldsymbol{\xi},\boldsymbol{\lambda})&=E_I(\mathbf{R})+\xi_1\Delta E_{IJ}(\mathbf{R})+\xi_2 H_{IJ}^{QQ}(\mathbf{R})\\&\quad+\sum_{i=1}^{N^{\rm con}}\lambda_i K_i(\mathbf{R}).\end{aligned}\tag{2.18}$$

Minimizing $L(\mathbf{R},\boldsymbol{\xi},\boldsymbol{\lambda})$ with respect to $\mathbf{R}$, $\boldsymbol{\xi}$, and $\boldsymbol{\lambda}$ through second order leads to the following Newton-Raphson equations:

$$\begin{pmatrix}\boldsymbol{Q}^{IJ}(\bar{\mathbf{R}},\boldsymbol{\xi},\boldsymbol{\lambda}) & \mathbf{g}^{IJ}(\mathbf{R}) & \mathbf{h}^{IJ}(\mathbf{R}) & \mathbf{k}^{IJ}(\mathbf{R})\\ \mathbf{g}^{IJ}(\mathbf{R})^{\dagger} & 0 & 0 & \mathbf{0}\\ \mathbf{h}^{IJ}(\mathbf{R})^{\dagger} & 0 & 0 & \mathbf{0}\\ \mathbf{k}^{IJ}(\mathbf{R})^{\dagger} & \mathbf{0}^{\dagger} & \mathbf{0}^{\dagger} & \mathbf{0}\end{pmatrix}\begin{pmatrix}\delta\mathbf{R}\\ \delta\xi_1\\ \delta\xi_2\\ \delta\boldsymbol{\lambda}\end{pmatrix}=-\begin{pmatrix}\mathbf{g}^I(\mathbf{R})+\xi_1\mathbf{g}^{IJ}(\mathbf{R})+\xi_2\mathbf{h}^{IJ}(\mathbf{R})+\sum_i\lambda_i\mathbf{k}^i(\mathbf{R})\\ \Delta E_{IJ}(\mathbf{R})\\ 0\\ \mathbf{K}(\mathbf{R})\end{pmatrix}\tag{2.19}$$

(2.19a)–(2.19d)

where $\delta\mathbf{R}=\mathbf{R}'-\mathbf{R}$, $\delta\boldsymbol{\lambda}=\boldsymbol{\lambda}'-\boldsymbol{\lambda}$, $\delta\boldsymbol{\xi}=\boldsymbol{\xi}'-\boldsymbol{\xi}$, $k_\alpha^i(\mathbf{R})=\partial K_i(\mathbf{R})/\partial R_\alpha$, and $\boldsymbol{Q}^{IJ}(\mathbf{R})$ is a second derivative matrix, $Q_{\alpha\beta}^{IJ}(\mathbf{R})=\partial^2 L(\mathbf{R},\xi,\lambda)/\partial R_\alpha\partial R_\beta$ (Manaa and Yarkony, 1993b).

Equation (2.19) is the basis of the computational tools used in this review to study the conical intersections of two states of the same symmetry, and thus its use merits some discussion. The appearance of $\boldsymbol{Q}^{IJ}(\bar{\mathbf{R}},\boldsymbol{\xi},\boldsymbol{\lambda})$ rather than $\boldsymbol{Q}^{IJ}(\mathbf{R},\boldsymbol{\xi},\boldsymbol{\lambda})$ in Eq. (2.19) reflects the procedure used for its solution. Equation (2.19) is solved iteratively until $\delta\mathbf{R}=\delta\boldsymbol{\xi}=\delta\boldsymbol{\lambda}=\mathbf{0}$. For the algorithm to be numerically viable, the quantities that appear on the right-hand side of Eq. (2.19) must be readily available at each $\mathbf{R}$. Efficient evaluation of these quantities is achieved using analytic

gradient techniques and has been reviewed elsewhere (Yarkony, 1995). $\boldsymbol{Q}^{IJ}(\mathbf{R},\boldsymbol{\xi},\boldsymbol{\lambda})$ is, however, costly to evaluate, requiring at present the use of divided difference techniques (Hettema and Yarkony, 1995). Thus it is not evaluated at each $\mathbf{R}$. Since the solution of Eq. (2.19) requires only the exact evaluation of the right-hand side, approximations for $\boldsymbol{Q}^{IJ}(\mathbf{R},\boldsymbol{\xi},\boldsymbol{\lambda})$ that do not adversely affect the rate of convergence to a solution are quite acceptable.

Equation (2.19) has $2+N^{\rm con}$ zero-diagonal elements, so that its desired solutions are saddle points in the total space of $\mathbf{R},\boldsymbol{\xi},\boldsymbol{\lambda}$. The dependence $E_I(\mathbf{R})$ on $\mathbf{R}$ in the subspace $\mathbf{R}^{\perp}$ of internal coordinates orthogonal to the span of $\mathbf{g}^{IJ}$, $\mathbf{h}^{IJ}$, and $\mathbf{k}_i$, $i=1-N^{\rm con}$, can be deduced from the projection of the exact $\boldsymbol{Q}^{IJ}$ onto that subspace. Local minima of $E_I(\mathbf{R})$ in $\mathbf{R}^{\perp}$ correspond to a positive-definite projection of $\boldsymbol{Q}^{IJ}$ (Fletcher, 1981). $\mathbf{R}_{\rm mex}$, the point on the surface of intersection with the lowest value of $E_I(\mathbf{R})$, is referred to as the minimum-energy crossing point.

Equations (2.19b) and (2.19c) are identical to Eqs. (2.17a) and (2.17b) and therefore enforce the degeneracy, while Eq. (2.19d) enforces the geometrical constraints. Eq. (2.19a) achieves the energy minimization. These observations lead to additional ways of using Eq. (2.19). The observation that Eq. (2.19d) enforces the geometrical constraints can be used to predict (approximately) the location of neighboring points on the surface of conical intersections. (Manaa and Yarkony, 1993b). This feature is routinely used in characterizing a particular region of a surface of conical intersection. If $\boldsymbol{Q}^{IJ}$ is replaced by a (diagonal) matrix with large positive diagonal elements, the energy minimization aspect of the algorithm will be damped and a point on the surface of conical intersection near $\mathbf{R}_0$ will be located. This latter aspect of the use of Eq. (2.19) will be considered in Sec. III.D.

2. Conical, glancing, and avoided intersections

An alternative approach for characterizing surfaces of conical intersection, which is generally applicable but has found its principle application in triatomic systems (Manaa and Yarkony, 1990, 1992; Kuntz *et al.*, 1994), seeks to find minima in $\Delta E_{IJ}(\mathbf{R})^2$. The algorithm follows from the straightforward observation that surfaces of conical intersections represent a class of solutions of the equation $(\partial/\partial R_\alpha)\Delta E_{IJ}(\mathbf{R})^2 \equiv G_\alpha^{IJ}(\mathbf{R}) = 2g_\alpha^{IJ}(\mathbf{R})\Delta E_{IJ}(\mathbf{R}) = 0$. Three classes of solutions to this equation exist, conical intersections for which $\Delta E_{IJ}(\mathbf{R})=0$, $g_\alpha^{IJ}(\mathbf{R})\neq 0$ and two classes of solutions for which the slopes of the potential-energy surfaces are parallel: those for which $\Delta E_{IJ}(\mathbf{R})=0$ and $g_\alpha^{IJ}(\mathbf{R})=0$ (Renner-Teller or glancing intersections); and those for which $\Delta E_{IJ}(\mathbf{R})\neq 0$, but $g_\alpha^{IJ}(\mathbf{R})=0$. This latter class of extrema will be referred to as *avoided intersections* for reasons discussed further below. This situation differs from that of the preceding algorithm, for which the only solutions are conical intersections.

The solution of $G_\alpha^{IJ}(\mathbf{R})=0$ can be accomplished using a Newton-Raphson procedure,

$$\mathbf{F}^{IJ}(\mathbf{R}_0)\,\delta = -\mathbf{G}^{IJ}(\mathbf{R}_0), \tag{2.20}$$

where $F^{IJ}(\mathbf{R}_0)$ is the second derivative or hessian matrix given by

$$\begin{aligned} F_{\alpha\beta}^{IJ}(\mathbf{R}_0) &= \frac{\partial}{\partial R_\alpha} G_\beta^{IJ}(\mathbf{R}_0) \\ &= 2g_\alpha^{IJ}(\mathbf{R}_0)g_\beta^{IJ}(\mathbf{R}_0) + 2\Delta E_{IJ}(\mathbf{R}_0) \\ &\quad \times \frac{\partial}{\partial R_\alpha} g_\beta^{IJ}(\mathbf{R}_0). \end{aligned} \tag{2.21}$$

The key issue in the use of Eq. (2.20) is the subspace of internal coordinates in which this equation is to be solved. In triatomic systems Eq. (2.20) can be employed using orthogonal Jacobi coordinates $\mathbf{j}=(R,r,\gamma)$. In accordance with the dimension of the surface of conical intersection, a preassigned coordinate j_1 is fixed at a particular value and Eq. (2.20) solved in the remaining two-dimensional space. In this way the surface (here a seam) of intersection is mapped out as a function of j_1. This procedure, which has been successfully applied to determine seams of conical intersection in triatomic systems (Manaa and Yarkony, 1990, 1992) is entirely adequate as long as $\hat{j}_i$, the unit vector in the direction of j_i, has a nonzero projection onto g-$h^{\perp}$. If this is not the case, the procedure will fail. This pitfall can be avoided by examining the eigenvalues of the hessian matrix $F^{IJ}(\mathbf{R}_0)$ at any point on the surface of intersection. The tangent to the surface of intersection will correspond to the eigenvector corresponding to the zero eigenvalue for this matrix. A very careful analysis of this situation has been provided by Kuntz and co-workers (Kuntz *et al.*, 1994). This point is discussed from an alternative perspective in Sec. III.A.2.

When $\Delta E_{IJ}(\mathbf{R})$ is never 0, or not 0 on a domain, solutions to Eq. (2.20) may still exist on that domain provided $g_\alpha^{IJ}(\mathbf{R})=0$, where the components of $\mathbf{g}^{IJ}(\mathbf{R})$ are restricted to (projected onto) the domain under consideration. We shall refer to such solutions as points of *avoided intersection*. There appears to be no natural definition for this domain or even its dimension. In the past we have found it useful, in triatomic systems, to take the domain to be orthogonal to a particular internal Jacobi coordinate and thereby determine an avoided-crossing seam (Gallo and Yarkony, 1986; Manaa and Yarkony, 1993b). This leads to a simple analogy between seams of conical intersections and avoided intersections. Seams of avoided intersection have been determined for the nonadiabatic quenching reactions $M(^2\mathrm{P})+\mathrm{HCl}\rightarrow M\mathrm{Cl}+\mathrm{H}$ for M=Na (Gallo and Yarkony, 1986) and Li (Manaa and Yarkony, 1993b) using the Jacobi coordinate $R(M\text{-HCl})$ as the seam parameter. Subsequent studies (Eaker, 1990) of the dynamics of the M=Na reaction found that the propensity for an electronically nonadiabatic transition was most significant in the vicinity of the seam, in accord with intuitive notions. It is important to reemphasize, however, that the surface

of intersection is a unique property of the two surfaces in question. The surface of avoided intersection depends, however, on the domain chosen.

D. Properties of adiabatic wave functions near surface intersections: A comparison of conical and Renner-Teller intersections

Not all intersections of potential-energy surfaces produce the same effect on the adiabatic electronic wave functions. Conical intersections and Renner-Teller intersections exhibit characteristic differences. The geometric phase effect arises for a conical intersection but not for a Renner-Teller intersection. As these examples have important implications for the numerical studies in Sec. III, the differences between conical and Renner-Teller intersections are briefly reviewed below.

1. Electronic structure

Equation (2.14) can be used to consider the (phase) behavior of the real-valued adiabatic wave functions along closed loops surrounding an intersection point. This matter has been addressed by Longuet-Higgins (1961) and Mead (1983). Note from Eq. (2.14) that the phase behavior of the wave function follows its behavior in Q space, since $[\boldsymbol{H}^{PP}(\mathbf{R})-\boldsymbol{I}E_I(\mathbf{R})]^P\mathbf{C}(\mathbf{R})=-\boldsymbol{H}^{PQ}(\mathbf{R})^Q\mathbf{c}(\mathbf{R})$. The Q-space portion of the wave function is determined from the effective eigenvalue problem:

$$[\boldsymbol{H}^{\text{eff}}-\boldsymbol{I}E_I(\mathbf{R})]^Q\mathbf{c}(\mathbf{R})=\mathbf{0} \tag{2.22a}$$

where

$$\boldsymbol{H}^{\text{eff}}=\boldsymbol{H}^{QQ}+\boldsymbol{H}^{QP}[\boldsymbol{I}E_I(\mathbf{R})-\boldsymbol{H}^{PP}]^{-1}\boldsymbol{H}^{PQ}. \tag{2.22b}$$

$\boldsymbol{H}^{\text{eff}}$ can be expanded perturbatively. This has been done by Mead for C_{3v}, symmetry-required, conical intersections (Mead, 1983). For the presented discussion a phenomenological approach is adequate. $\boldsymbol{H}^{\text{eff}}$ can be represented as

$$\begin{pmatrix} H+V_R & V_I \\ V_I & H-V_R \end{pmatrix}, \tag{2.23}$$

which can be diagonalized by the orthogonal transformation

$$\mathbf{T}(\phi)=\begin{pmatrix} \cos\phi & -\sin\phi \\ \sin\phi & \cos\phi \end{pmatrix}, \tag{2.24}$$

where $\tan 2\phi=-V_I/V_R$. V_I and V_R can be expanded in power series in the displacements, denoted x,y:

$$V_R=ax+by+cx^2+2exy+dy^2\ldots, \tag{2.25a}$$

$$V_I=\bar{a}x+\bar{b}y+\bar{c}x^2+2\bar{e}xy+\bar{d}y^2\ldots\ . \tag{2.25b}$$

The origin $(x,y)=(0,0)$ is a point of intersection. Closed loops around the origin are straightforwardly defined in terms of polar coordinates (ρ,θ) given by $x=\rho\cos\theta$, $y=\rho\sin\theta$. From Eq. (2.15) the linear terms in Eq. (2.25) could be determined from $\mathbf{h}^{IJ}(\mathbf{R}_x)$ and $\mathbf{g}^{IJ}(\mathbf{R}_x)$, whereas the quadratic terms contain contributions from both the P space and the Q space.

For a quadratic Jahn-Teller-like Hamiltonian,

$$-V_R=2(v^Rx-v^Iy)+2[v^r(x^2-y^2)+v^i2xy], \tag{2.26a}$$

$$V_I=2(v^Ry+v^Ix)+2[-v^r2xy+v^i(x^2-y^2)]. \tag{2.26b}$$

For a Renner-Teller Hamiltonian, the linear terms are absent, by symmetry (Longuet-Higgins, 1961). We define $(v^{(j)},\eta^{(j)})$, $j=1,2$ such that $[v^R=v^{(1)}\cos\eta^{(1)}$, $v^I=v^{(1)}\sin\eta^{(1)}]$ and $[v^r=v^{(2)}\cos\eta^{(2)}$, $v^i=v^{(2)}\sin\eta^{(2)}]$. Then

$$\tan 2\phi=\frac{v^{(1)}\rho\,\sin(\theta+\eta^{(1)})+v^{(2)}\rho^2\sin(-2\theta+\eta^{(2)})}{v^{(1)}\rho\,\cos(\theta+\eta^{(1)})+v^{(2)}\rho^2\cos(-2\theta+\eta^{(2)})} \tag{2.27}$$

so that $\mathbf{T}(\phi[\rho,\theta])\equiv\mathbf{T}(\rho,\theta)=-\mathbf{T}(\rho,\theta+2\pi)$ for ρ small, and $\mathbf{T}(\rho,\theta)=+\mathbf{T}(\rho,\theta+2\pi)$ for ρ large. That is, there is a change in sign of the real-valued electronic wave functions transported around a circle with small ρ, but no such change for ρ large.

This simple analysis illustrates two important points concerning the geometric phase effect and surface intersections. First, the geometric phase effect is present for (linear) Jahn-Teller-type (conical) intersections but not for the (quadratic) Renner-Teller-type intersections. Secondly, a sign change in the real-valued wave function may not be observed for all closed loops surrounding a conical intersection. It is instructive to consider further these observations.

To see that there should be no geometric phase effect in a Renner-Teller system, observe that in the case of the Renner-Teller intersection the coordinate θ corresponds to an *overall* molecular rotation, rather than an internal motion as in the Jahn-Teller or conical intersection case. The real-valued wave functions in this case are of A' and A'' symmetry in the C_s point group and cannot mix, following instead the plane of the bent molecule as it is rotated (Longuet-Higgins, 1961).

The absence of a change in phase for a Hamiltonian defined by Eq. (2.26) for large ρ can be explained with the help of Fig. 4. This figure illustrates what happens when the radius of a closed loop increases from ρ_1, enclosing m points of conical intersection, to ρ_2, enclosing $m+1$ points of conical intersection. Each conical intersection point induces a geometric phase effect, so that if $\mathbf{T}(\rho_1,\theta)=-\mathbf{T}(\rho_1,\theta+2\pi)$ then $\mathbf{T}(\rho_2,\theta)=+\mathbf{T}(\rho_2,\theta+2\pi)$. Thus when a wave function is transported around a closed loop that encloses an odd (even) number of conical intersection points there will (will not) be a sign change. It is straightforward to see that this occurs for the Hamiltonian defined by Eq. (2.26). The eigenvalues are

$$\varepsilon^{\pm}=H\pm\sqrt{(v^{(1)}\rho)^2+(v^{(2)}\rho^2)^2+2v^{(1)}v^{(2)}\rho^3\cos(3\theta+\eta^{(1)}-\eta^{(2)})}. \tag{2.28}$$

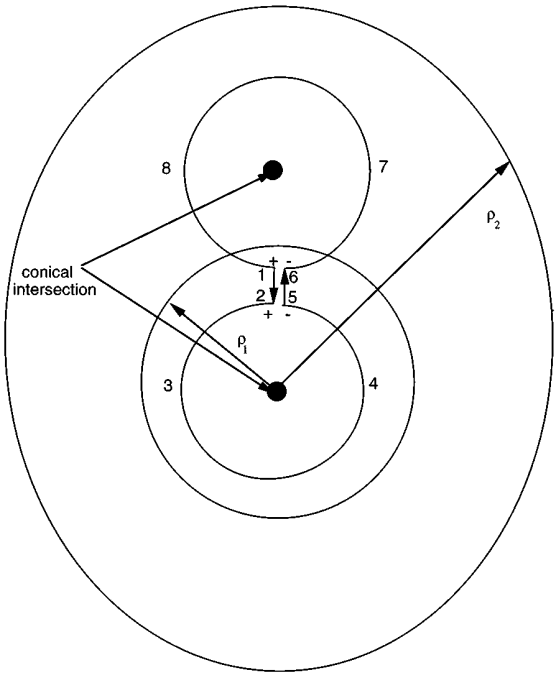

FIG. 4. Effect of additional conical intersection points on the geometric phase effect, after Mead and Truhlar (1979). Closed loops 6781 and 2345 each contain one point of conical intersection and exhibit the geometric phase effect. As a consequence the closed loop 123456781, containing two conical intersections, does not exhibit the geometric phase effect. These loops can be continuously distorted, without encountering additional points of conical intersection, to circular g-h paths with radii ρ_1 and ρ_2, respectively.

As observed by Zwanzinger and Grant, there are four degenerate eigenvalues, one at $\rho=0$ and three more at the common radius $\rho=v^{(1)}/v^{(2)}$ with $3\theta+\eta^{(1)}-\eta^{(2)}=(2n+1)\pi$, $n=0,1,2$.

2. Dynamics

To see the implications of the above differences for nuclear dynamics, consider the linear Jahn-Teller and quadratic Renner-Teller models described. Note that this approximate treatment neglects such effects as the spin-orbit interaction (Pople, 1960; Longuet-Higgins, 1961; Ham, 1987) and overall molecular rotation (Jungen and Merer, 1976), which would be present in real systems. Assume, following Longuet-Higgins (1961), that the ρ dependence of the electronic wave functions is subordinate to the θ dependence, that is, $\Psi_I(\mathbf{r};\rho,\theta)\sim\Psi_I(\mathbf{r};\theta)$ and $\Psi_J(\mathbf{r};\rho,\theta)\sim\Psi_J(\mathbf{r};\theta)$, and note that

$$\frac{\partial}{\partial x}=\cos\theta\,\frac{\partial}{\partial\rho}-\frac{\sin\theta}{\rho}\,\frac{\partial}{\partial\theta}, \tag{2.29a}$$

$$\frac{\partial}{\partial y}=\sin\theta\,\frac{\partial}{\partial\rho}+\frac{\cos\theta}{\rho}\,\frac{\partial}{\partial\theta}. \tag{2.29b}$$

In the Jahn-Teller case, $A_I(\mathbf{R})=A_J(\mathbf{R})=\theta/2$, so that Eq. (2.4b) gives $\tilde{\Psi}_I(\mathbf{r};\theta)=e^{i\theta/2}\Psi_I(\mathbf{r};\theta)$ and $\tilde{\Psi}_J(\mathbf{r};\theta)=e^{i\theta/2}\Psi_J(\mathbf{r};\theta)$. It is then readily verified that ∇A_I is singular at the origin, that $\oint\nabla A_I\cdot d\mathbf{R}=\pi$, and thus that $\nabla\times\nabla A_I=\pi\delta(x)\delta(y)$, as discussed following Eq. (2.12). For the linear Jahn-Teller effect, $E_I(\mathbf{R})$—which is generally a function of both ρ and θ—depends only on ρ. Thus, for the linear Jahn-Teller problem, Eq. (2.7b) for the *single-valued* vibrational wave functions $\chi_I(\rho,\theta)$ and $\chi_J(\rho,\theta)$ becomes

$$\begin{pmatrix} \frac{1}{2\mu\rho^2}\left[1/4+\left(-i\rho\,\frac{\partial}{\partial\rho}\right)^2+\left(-i\,\frac{\partial}{\partial\theta}+\frac{1}{2}\right)^2\right]+E_I(\rho) & \frac{i}{2\mu\rho^2}\left(-i\,\frac{\partial}{\partial\theta}+\frac{1}{2}\right) \\ \frac{-i}{2\mu\rho^2}\left(-i\,\frac{\partial}{\partial\theta}+\frac{1}{2}\right) & \frac{1}{2\mu\rho^2}\left[\frac{1}{4}+\left(-i\rho\,\frac{\partial}{\partial\rho}\right)^2+\left(-i\,\frac{\partial}{\partial\theta}+\frac{1}{2}\right)^2\right]+E_J(\rho) \end{pmatrix}\begin{pmatrix}\chi_I\\ \chi_J\end{pmatrix} = E\begin{pmatrix}\chi_I\\ \chi_J\end{pmatrix}. \tag{2.30a}$$

The term $1/(8\mu\rho^2)$ is the singular, adiabatic correction discussed in Sec. II.A.

In the Renner-Teller case, $A_I(\mathbf{R})=A_J(\mathbf{R})=0$ and $E_I(\mathbf{R})$ is a function only of ρ^2, so that $\tilde{\Psi}_I(\mathbf{r};\theta)=\Psi_I(\mathbf{r};\theta)$ and $\tilde{\Psi}_J(\mathbf{r};\theta)=\Psi_J(\mathbf{r};\theta)$ and Eq. (2.8) becomes

$$\begin{pmatrix} \frac{1}{2\mu\rho^2}\left[1+\left(-i\rho\,\frac{\partial}{\partial\rho}\right)^2+\left(-i\,\frac{\partial}{\partial\theta}\right)^2\right]+E_I(\rho^2) & \frac{i}{\mu\rho^2}\left(-i\,\frac{\partial}{\partial\theta}\right) \\ \frac{-i}{\mu\rho^2}\left(-i\,\frac{\partial}{\partial\theta}\right) & \frac{1}{2\mu\rho^2}\left[1+\left(-i\rho\,\frac{\partial}{\partial\rho}\right)^2+\left(-i\,\frac{\partial}{\partial\theta}\right)^2\right]+E_J(\rho^2) \end{pmatrix}\begin{pmatrix}\chi_I\\ \chi_J\end{pmatrix} = E\begin{pmatrix}\chi_I\\ \chi_J\end{pmatrix}. \tag{2.30b}$$

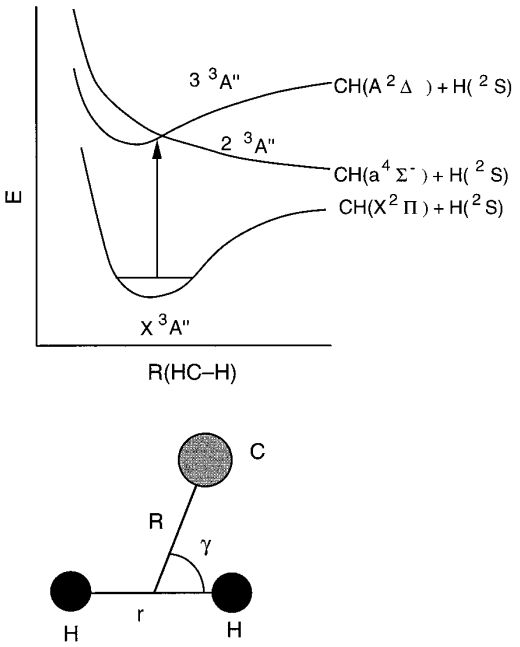

FIG. 5. CH_2: Schematic representation of $1,2,3^3A''$ electronic states of, and Jacobi coordinates for, methylene.

In deriving Eqs. (2.30a) and (2.30b), we observed that

$$\frac{\partial}{\partial\theta}\Psi_I = -\Psi_J \frac{\partial\phi}{\partial\theta}$$

and

$$\frac{\partial}{\partial\theta}\Psi_J = \Psi_I \frac{\partial\phi}{\partial\theta},$$

which follows from Eq. (2.24) [neglecting the geometry dependence of the basis states in Eq. (2.24)] and that $(\partial\phi/\partial\theta)=1/2$ (Jahn-Teller) or $(\partial\phi/\partial\theta)=1$ (Renner-Teller), which follows from Eq. (2.27).

Equations (2.30a) and (2.30b) will not be analyzed in detail. They were considered by Longuet-Higgins in his seminal description of the Jahn-Teller and Renner-Teller effects in molecular spectroscopy (Longuet-Higgins, 1961). Quite recently, moreover, related Hamiltonians in triatomic systems have been analyzed using wave-packet techniques (Schön and Köppel, 1994) and gauge-potential approaches (Wu *et al.*, 1994; Kendrick and Pack, 1996a, 1996b). The key point here is the θ dependence of the "vibrational" wave functions $\chi_J(\rho,\theta)$, which, being single valued, can be expanded in a basis of $e^{\pm in\theta}$ for n an integer. Since $e^{-i\theta/2}(\partial/\partial\theta)e^{i\theta/2}\chi_J(\rho,\theta) = [(\partial/\partial\theta)+i/2]\chi_J(\rho,\theta)$, this expansion in integer n becomes an expansion in $n+1/2$ for the Jahn-Teller problem while remaining an expansion in n for the Renner-Teller problem. In the present case $-i(\partial/\partial\theta)\boldsymbol{I}$ commutes with the Hamiltonian, so that $(n+1/2)$ is a good quantum number for the linear Jahn-Teller problem and n is a good quantum number for the Renner-Teller problem. This essential difference between the Renner-Teller and Jahn-Teller problems can be viewed as a direct consequence of the geometric phase effect. The analysis of Sec. III.D.1 shows that the quadratic Jahn-Teller problem would not exhibit half-integer quantization if the nuclear motion were restricted to the large-ρ region. Recently there has been considerable experimental effort devoted to determining the type of quantization exhibited in X_3-like Jahn-Teller systems (Delacrétaz *et al.*, 1986; Zwanziger and Grant, 1987; Ernst and Rakowsky, 1995a, 1995b).

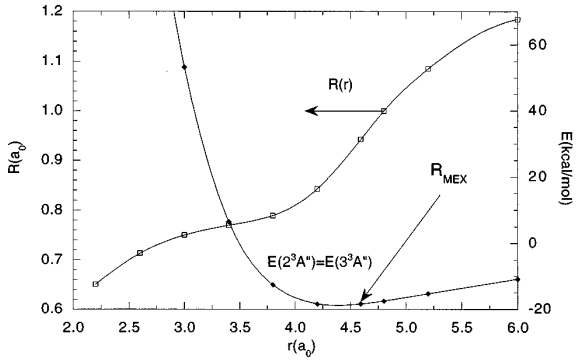

FIG. 6. CH_2: R left-hand ordinate and $E_{2^3A''}=E_{3^3A''}$ right-hand ordinate along the $2^3A''$-$3^3A''$ seam of conical intersections parametrized by $r=R(\mathrm{HH})$. The Jacobi coordinates R,r are defined in Fig. 5.

While the preceding treatment is only approximate, it illustrates the essential features of recent treatments of the geometric phase problem in $H+H_2$ molecular scattering (Lepetit *et al.*, 1990; Kuppermann and Wu, 1993; Wu and Kuppermann, 1993, 1995). In these treatments hyperspherical coordinates (Johnson, 1980) are used. For equal mass systems, closed paths around the seam of a conical intersection correspond to motion in the single hyperspherical coordinate ϕ_λ (Kuppermann and Wu, 1993). In these instances the simple form of the gauge phases used above is applicable.

III. CONICAL INTERSECTIONS IN MOLECULAR SYSTEMS

Analysis of the nuclear dynamics in the vicinity of Jahn-Teller and Renner-Teller intersections is a difficult task. On the other hand, the location of the conical intersection and the determination of the g-h plane are made completely straightforward as a consequence of molecular point-group symmetry. This section addresses, from a practical perspective, the location of conical intersections and the determination of the g-h plane when molecular point-group symmetry does not determine these quantities. In this situation the effect of a conical intersection is particularly diabolical, since its existence is difficult to anticipate, making efficient numerical procedures to identify such situations highly desirable. While the condition for a conical intersection, $\Delta E_{IJ}=0$, can never be achieved exactly in a numerical computation, for points denoted as conical intersection points in this work ΔE_{IJ} is quite small, generally less than the 0.5 cm^{-1}.

For the Berry phase effect to be evinced in the nuclear dynamics, an energetically accessible g-h path on the lower adiabatic potential-energy surface is required. For a circular g-h path on the lower adiabatic

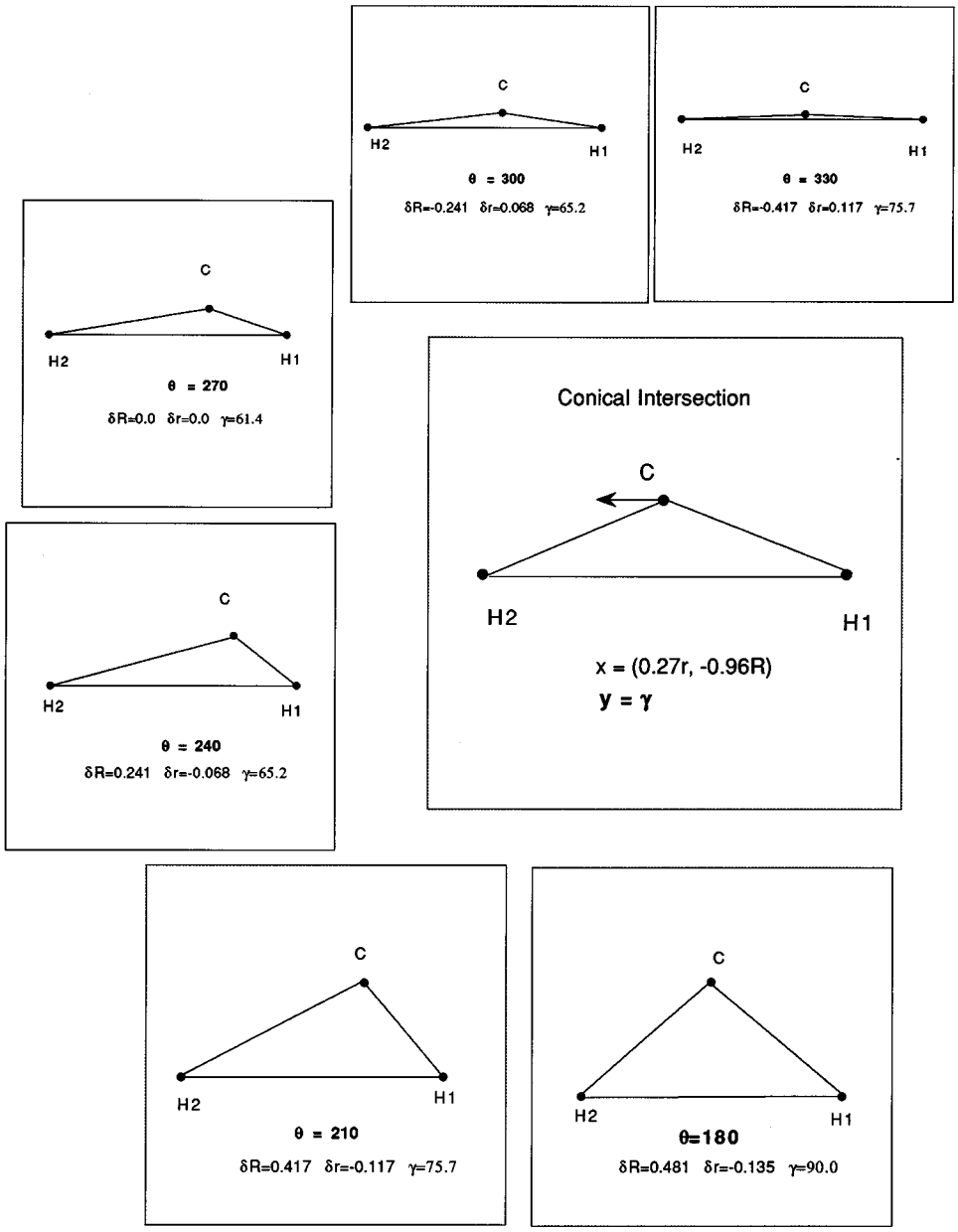

FIG. 7. CH_2: Nuclear configurations and Jacobi coordinates for indicated values of θ with ρ=0.5. The origin, ρ=0, is the conical intersection point $\mathbf{R}_{\text{mex}}$. $\delta R \equiv R - R_{\text{mex}}$. $\delta r \equiv r - r_{\text{mex}}$. The normalized $\mathbf{g}^{IJ}$ and $\mathbf{h}^{IJ}$ directions, x and y, respectively, are given in the central figures and indicated pictorially by arrows attached to the atoms.

potential-energy surface, it might be expected (at least near the conical intersection point) that the energy would be relatively constant along the path and *decrease* as its radius increased. However, this need not be the case. The diagonal offset term H in Eq. (2.23) and higher-order contributions can alter this conclusion, providing an energetic barrier that limits the significance of the geometric phase effect. Further, the discussion in Sec. II.D illustrates that the sign change in the adiabatic wave function may not occur for all g-h paths, so that behavior of the wave functions along these paths should also be considered.

The most convincing approach for establishing the phase behavior of the adiabatic wave function would proceed as follows: compute using nonorthogonal orbital techniques, $O_i = \langle \Psi_I(\mathbf{r};\mathbf{R}_i) | \Psi_I(\mathbf{r};\mathbf{R}_{i+1}) \rangle_{\mathbf{r}}$ for $i = 1, N-1$, where the $\mathbf{R}_i$ describe a circular g-h path with $\mathbf{R}_1 = \mathbf{R}_N$; require $1 > O_i \gg 0$; and finally compute $\langle \Psi_I(\mathbf{r};\mathbf{R}_1) | \Psi_I(\mathbf{r};\mathbf{R}_N) \rangle_{\mathbf{r}}$, which must be ± 1. This ideal procedure would be possible, since the path does not go through a conical intersection, but it is quite impractical from a computational perspective. Instead, simpler, but case-specific, diagnostics will be devised. In this regard the geometric phase effect has previously been analyzed in O_3 by Ruedenberg and co-workers (Xantheas *et al.*, 1990).

This section begins with an example of an accidental, but symmetry-allowed, conical intersection. The second

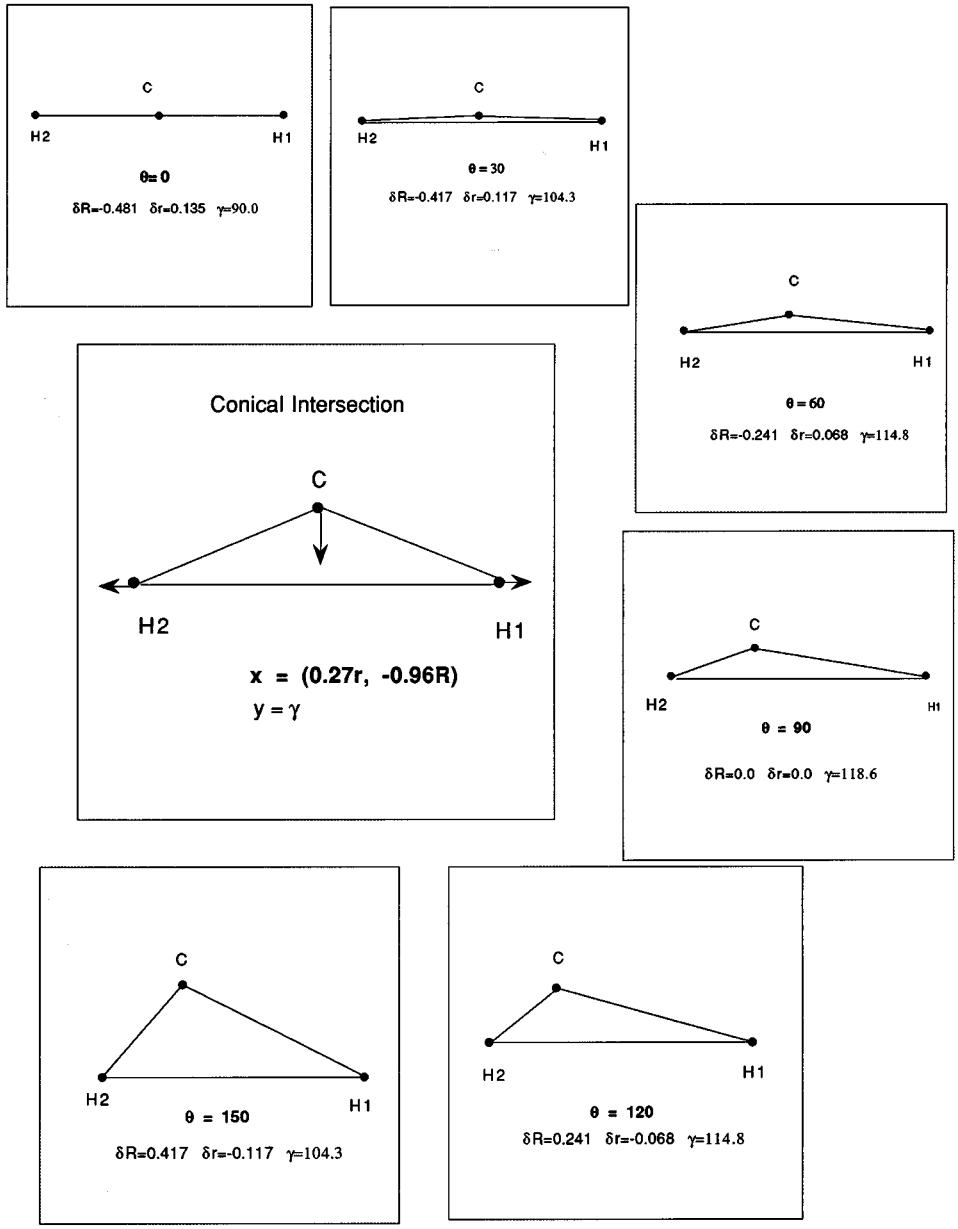

FIG. 7 (*Continued.*)

subsection considers a conical intersection of two states of the same symmetry, that is, a conical intersection in which symmetry plays no role. These examples are principally concerned with the geometric phase and its potential effect in single-surface, that is, adiabatic, processes. The topology of the potential-energy surface is considered along circular g-h paths. Decidedly different topologies are evinced for methylene and methyl mercaptan. The impact of these conical intersections on multisurface photodissociation is also discussed.

The third example considers an explicitly nonadiabatic, that is, multiple potential-energy surface, process facilitated by a conical intersection of two states of the same symmetry. It takes cognizance of the fact that the surface of conical intersection extends over a significant region of nuclear coordinate space and asks which regions of the surface of conical intersection can be sampled in a photodissociation process.

A. Conical intersections and the geometric phase in triatomic systems: The $2^3A''$, $3^3A''$ states of methylene

1. Introduction

The $2^3A''$ state of methylene, CH_2, exhibits a seam (a surface of dimension 1) of symmetry-allowed accidental conical intersections with the $3^3A''$ state for C_{2v} nuclear configurations for which the two states are of $^3A_2$ and $^3B_1$ symmetry. The portion of this seam of conical intersections near the equilibrium geometry of the ground

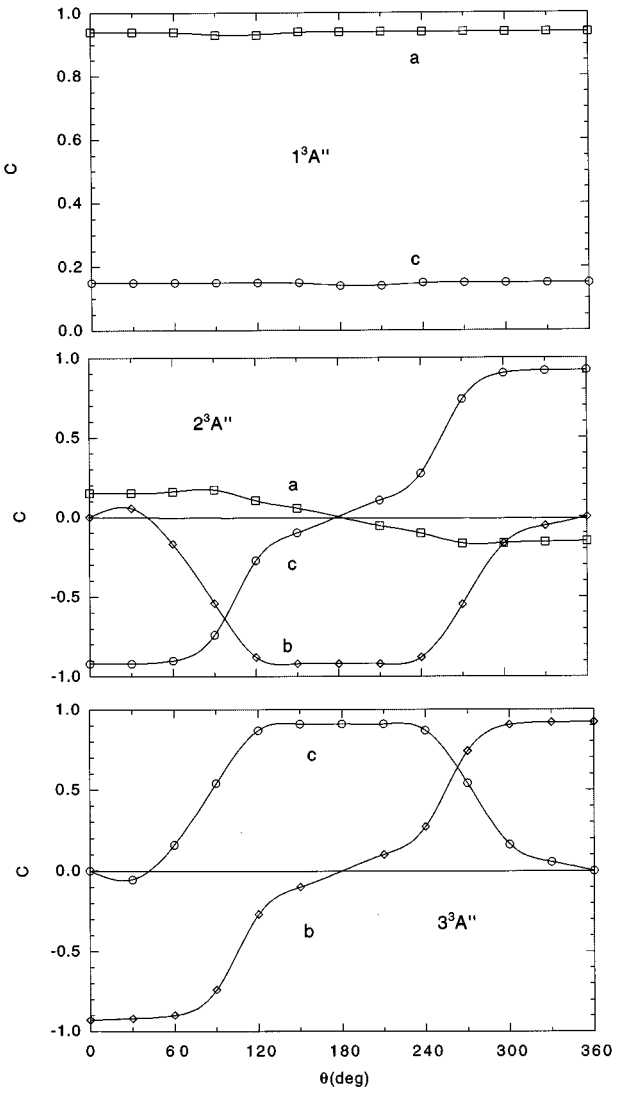

FIG. 8. CH_2: $\mathbf{c}^I(\mathbf{R})$ for $\mathbf{R}$ corresponding to ρ=0.1 and $0\leqslant\theta\leqslant360°$. The origin, ρ=0, is the conical intersection point $\mathbf{R}_{\text{mex}}$. $I=1^3A''$, $2^3A''$, and $3^3A''$ correspond to the upper, middle, and lower figures, respectively, and are denoted as Figs. 8(a), 8(b), 8(c) in the text. X designates c^I_{1X} [Eq. (2.4a)], where $1X$ denotes the CSF corresponding to electron configuration $3.1X$ in the text.

state, $1^3A''(1^3B_1)$, plays a key role in the nonadiabatic photochemical decomposition of CH_2 originating on the $3^3A''$ surface (Beärda *et al.*, 1992). The situation is illustrated schematically in Fig. 5. The geometric phase effect attributable to the $2^3A''$-$3^3A''$ conical intersection may also influence adiabatic processes on the $2^3A''$ surface. In this subsection the techniques described in Sec. II are used to explore these issues.

2. The *g-h* plane: Berry phase and energetics

Molecular configurations are described in terms of the orthogonal Jacobi coordinates, $\mathbf{R}\equiv(R,r,\gamma)$, where $r\equiv R(HH)$ and R,γ are the polar coordinates for the line connecting the carbon atom to the center of mass of the H_2 moiety; see Fig. 5. The seam of conical intersection were determined using Eq. (2.19). As the surface of intersection has dimension 1, it can be characterized by a single geometrical parameter. In order to choose this parameter, Eq. (2.19) was solved in the absence of any geometrical constraints, yielding the minimum-energy crossing point $\mathbf{R}_{\text{mex}}$=(0.94217, 4.5938, 90°). The tangent to the crossing seam at this point is $\mathbf{g}\text{-}\mathbf{h}^{\perp}(\mathbf{R}_{\text{mex}})$ $=0.2701\hat{R}+0.9628\hat{r}+0.0\hat{\gamma}\equiv\{0.2701,0.9628,0.0\}$, where the caret denotes a unit vector. Thus the tangent to the seam is largely parallel to $\hat{r}$. For this reason the seam of intersection was determined using $r=R(HH)\equiv\beta$ as the parameter, so that the seam and its tangent become $\mathbf{R}_x(\beta)=(R(\beta),\beta,\gamma(\beta))$ and $\mathbf{g}\text{-}\mathbf{h}^{\perp}[\mathbf{R}_x(\beta)]\equiv\mathbf{g}\text{-}\mathbf{h}^{\perp}(\beta)$, respectively. The slope of the tangent line at this point suggests, and subsequent calculations confirmed, that the determination of the seam would have been problematical using R as the parameter and impossible using γ. As noted in Sec. I.C.2, an alternative method for parametrizing a seam of intersection in triatomic systems can be found in Kuntz *et al.* (1994).

Equation (2.19) was then solved with $R(HH)=\beta$ constrained to its assigned value through Eq. (2.19d). Here Eq. (2.19a) becomes trivial when a single geometric constraint is imposed, since Eq. (2.19a) requires that $E_I(\mathbf{R})$ be a minimum except along three directions given by $\mathbf{g}^{IJ}$, $\mathbf{h}^{IJ}$, and $\mathbf{k}$. As these directions span the entire internal coordinate space, there are no internal coordinates left with which to minimize the energy.

The $2^3A''$-$3^3A''$ crossing seam, $\mathbf{R}_x(\beta)$, together with $E(2^3A'')=E(3^3A'')$ and $E(1^3A'')$ are depicted in Fig. 6. There it can be seen that the seam of intersection is a line, rather than a closed loop, covering the range $0\leqslant r\leqslant\infty$, with $\gamma\equiv90°$. The large r values correspond to $C(^3P)+2H(^2S)$. It should be noted that more complicated seams of intersection are possible involving combinations of symmetry-allowed and same-symmetry intersections. Such a situation has been reported in HCO^+ (Kuntz *et al.*, 1994).

The energy and wave functions were studied in the g-h plane at $\mathbf{R}_x(4.5938)=\mathbf{R}_{\text{mex}}$. From Eq. (2.19) it was found that the g-h plane could be defined by the unit vectors $\hat{x}\equiv\{0.9628,-0.2701,0.0\}$ and $\hat{y}\equiv\{0.0,0.0,1.0\}$. Note that, unlike the Jahn-Teller case, the g-h plane could not have been determined from symmetry considerations. The molecular motion along circular g-h paths is depicted in Fig. 7, using standard polar (ρ,θ) coordinates. (Coordinates are displayed for $\rho=0.5a_0$, but plotted for ρ=1.0 for clarity.) Note that $(\rho,180°-\theta)$ and $(\rho,180°+\theta)$ are mirror-image configurations, so that $E_I(\rho,180°+\theta)=E_I(\rho,180°-\theta)$, $0<\theta<180°$.

The geometric phase effect is illustrated in Figs. 8(a)–8(c), where the coefficients of the principal CSFs are plotted,

$$[1a'^2\cdots7a'^2 \quad 1a''^2 2a''^2] \quad 8a'^2 9a'^2 10a'^2 3a''^2, \tag{3.1a}$$

$$[1a'^2\cdots7a'^2 \quad 1a''^2 2a''^2] \quad 8a'^2 9a'^2 10a'^2 3a''^2 11a', \tag{3.1b}$$

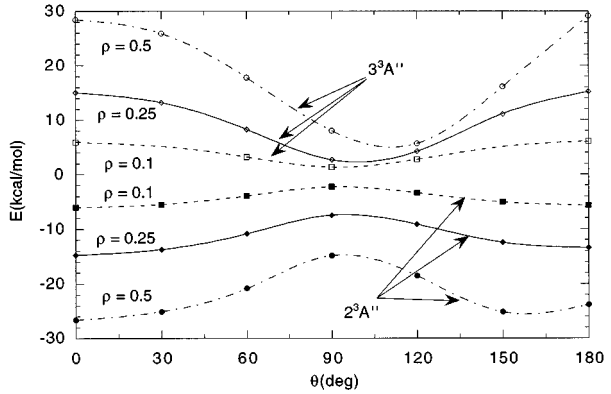

FIG. 9. CH_2: $E_{2^3A''}$ and $E_{3^3A''}$ for $0 \leqslant \theta \leqslant 180$, and ρ=0.1,0.25, $0.5a_0$. The origin, ρ=0, is the conical intersection point $\mathbf{R}_{\text{mex}}$.

$$[1a'^2 \cdots 7a'^2 \quad 1a''^2 2a''^2] \quad 8a'^2 9a'^2 10a'^2 3a''12a', \tag{3.1c}$$

for the $1,2,3^3A''$ states, respectively, along circular g-h paths with ρ=0.1. For Figs. 8(b) and 8(c), the sign change can be seen to "originate" from the behavior of the wave functions near θ=180°, where for each of the $2,3^3A''$ states the coefficients that are large for θ=0° pass through zero. This behavior should be contrasted with the virtual absence of a θ dependence for the $1^3A''$ state [Fig. 8(a)], for which a conical intersection does not exist.

Figure 9 considers the energetics along the circular g-h paths, reporting $E_{2^3A''}$ and $E_{3^3A''}$ for $0° \leqslant \theta \leqslant 180°$, and ρ=0.1,0.25,$0.5a_0$. It is important to observe that, for fixed θ, $E_{2^3A''}$ decreases while $E_{3^3A''}$ increases as ρ increases, consistent with a qualitatively conical structure.

3. Relation to inelastic scattering

The inelastic energy-transfer reaction

$$\text{H}(^2S) + \text{CH}(a^4\Sigma^-, v, N, e/f) \rightarrow \text{H}(^2S) + \text{CH}(a^4\Sigma^-, v', N', e'/f') \tag{3.2}$$

takes place on the $2^3A''$ potential-energy surface. Note that, although electronically excited, the $\text{CH}(a^4\Sigma^-)$ moiety is relatively long lived, with a lifetime greater than 1s (Hettema and Yarkony, 1994). It can be produced from $CHBr_3$ (Hou and Bayes, 1993), so that it can be used in laboratory experiments. The presence of the $2^3A''$-$3^3A''$ conical intersection may influence reaction (3.2) through the geometric phase effect. It is thus germane to ask under what circumstances g-h paths are energetically accessible. This question is addressed in Fig. 9, which reports the variation in energy along closed loops surrounding the lowest-energy conical intersection point. On the basis of the dissociation energy of CH_2 [D_0>4.23 eV] and T_e [$\text{CH}(a^4\Sigma^-)$]=5844 cm^{-1}, the lowest-energy conical intersection ($\mathbf{R}_{\text{mex}}$), 7.1 eV above the minimum on the 1^3B_1 potential energy surface, is approximately 2.1 eV above the $\text{CH}(a^4\Sigma^-)$+$\text{H}(^2S)$ asymptote (Yarkony, 1996b). The analogous value in the H_3 case, noted in the Introduction, is 2.7 eV. Thus from Fig. 9 it can be seen that an H atom with approximately 1.3 eV of energy could circumnavigate the conical intersection at ρ=0.5, providing the opportunity for the geometric phase effect to influence reaction (3.2).

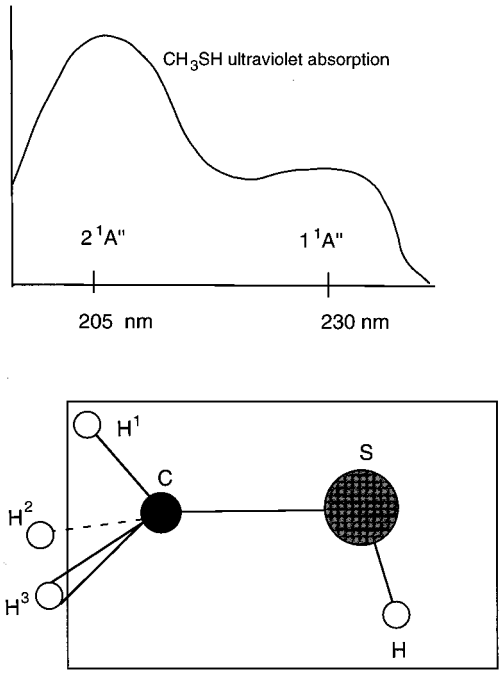

FIG. 10. CH_3SH: Schematic representation of the X^1A' state and the $1,2^1A''$ states of, and geometrical arrangement for, methyl mercaptan. $\Delta(I) \equiv I(\mathbf{R}_x) - I(\mathbf{R}_{\text{eq}})$, where I represents an internuclear parameter, $\mathbf{R}_x$ is the conical intersection point, and $\mathbf{R}_{\text{eq}}$ is the equilibrium geometry of the $1^1A'$ state discussed in the text.

4. Relation to photodissociation: The role of derivative couplings

The near-equilibrium photoexcitation process $X^3B_1 \rightarrow 3^3A''$, which has a large dipole moment (Yarkony, 1996b), is expected to lead to the nonadiabatic transition $3^3A'' \rightarrow 2^3A''$ owing to the funneling effect of the $2^3A''$-$3^3A''$ seam of conical intersections. Since a portion of the $2^3A''$-$3^3A''$ seam of conical intersection lies in the vicinity of the equilibrium geometry of the X^3B_1 state, the initially excited wave packet may span a closed path around a conical intersection. This will significantly complicate the description of the absorption process, $X^3B_1 \rightarrow 2,3^3A''$.

It may seem counterintuitive that the seam of conical intersections would play any role in the actual dynamics on the $3^3A''$ potential-energy surface, despite the local topology which would funnel a classical trajectory or quantum wave packet toward the seam. After all, the seam itself is of negligible volume as far as this same classical trajectory or quantum wave packet is concerned. This dilemma is resolved with the realization that the seam (surface) of conical intersections is at the center of a volume in which the probability of a nona-

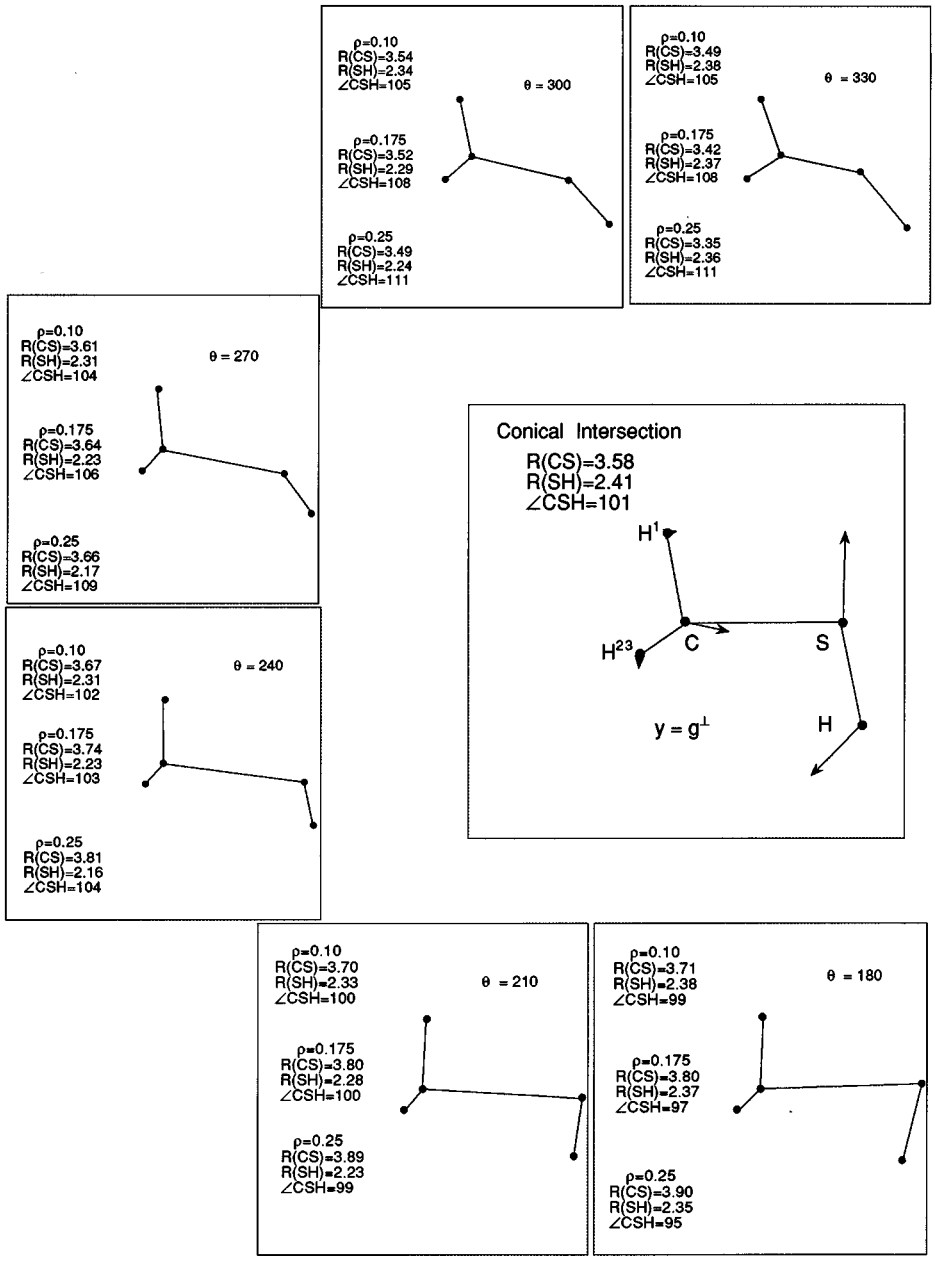

FIG. 11. CH_3SH: Nuclear configurations for indicated values of θ with ρ=0.25,0.175,0.10 (ρ=1.0 is plotted for emphasis), projected onto the Z=0 plane. H^2 and H^3 are superimposed. The origin, ρ=0, is the conical intersection point $\mathbf{R}_x$. The normalized $\tilde{\mathbf{g}}^{IJ}$ and $\mathbf{h}^{IJ}$ directions, y and x, respectively, are indicated pictorially in the central figures by arrows attached to the atoms.

diabatic transition is large. The breadth of the volume is determined by the derivative couplings. In this regard a well-studied nonadiabatic process is the electronic quenching reaction $Na(^2P)+H_2 \rightarrow Na(^2S)+H_2$. Derivative couplings have been determined, using *ab initio* wave functions by Yarkony (1986) and by Truhlar and co-workers (Truhlar *et al.*, 1982; Blais, Truhlar, and Garrett, 1983a) using diatomics in molecules wave functions, in the vicinity of a symmetry-allowed seam of conical intersections relevant to this reaction. An analysis of the propensity for a nonadiabatic transition as a funciton of nuclear coordinates has also been reported (Blais and Truhlar, 1983).

B. Conical intersections and the geometric phase in general polyatomic systems: The $1^1A''$,$2^1A''$ states of methyl mercaptan

1. Introduction

The ultraviolet absorption spectrum of methyl mercaptan,

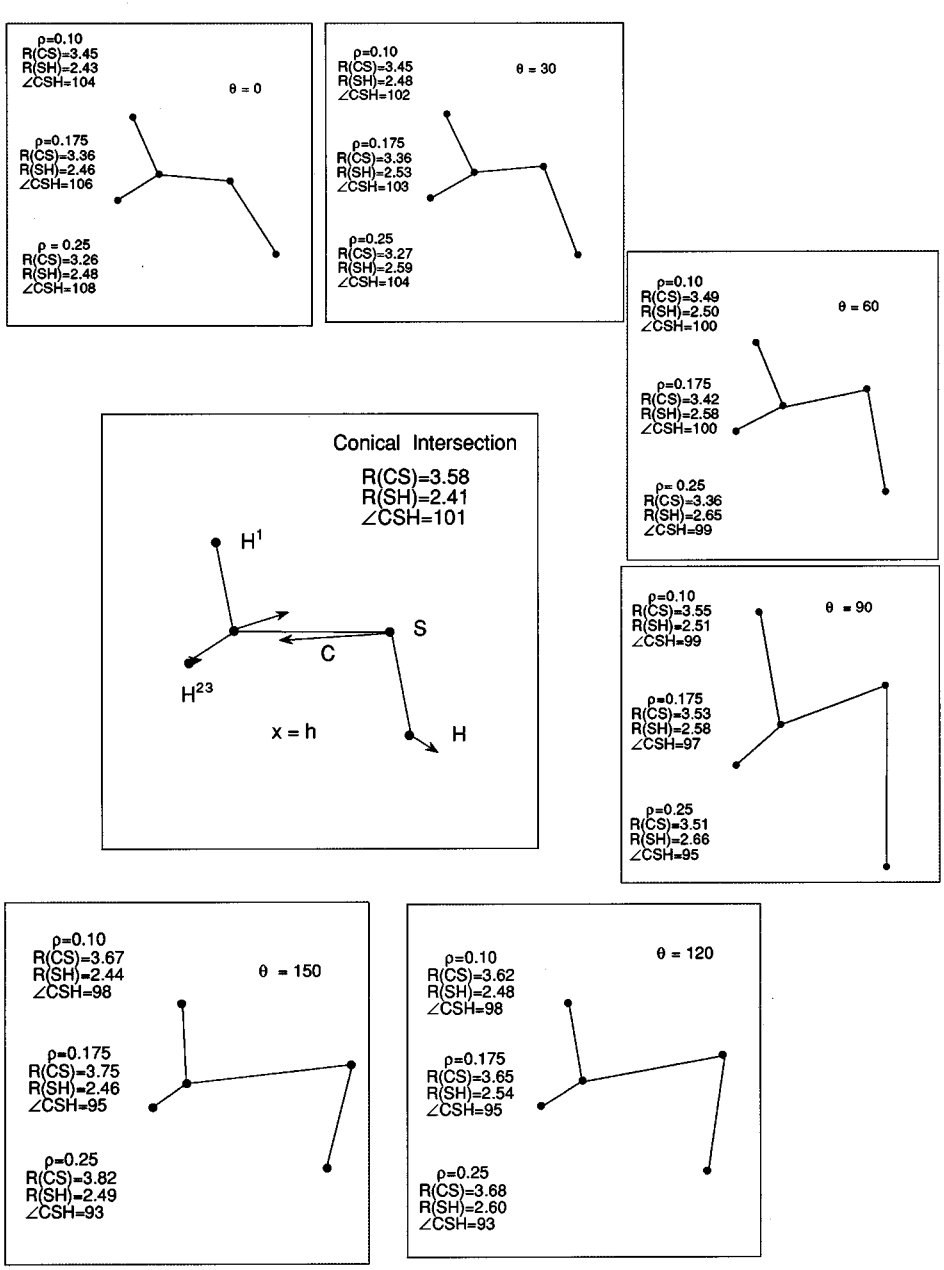

FIG. 11 (*Continued.*)

$$\mathrm{CH_3SH}(X^1A') + h\nu \rightarrow \mathrm{CH_3SH}(1,2^1A'') \rightarrow \mathrm{CH_3SH}(1^1A'') \rightarrow \mathrm{CH_3S{+}H \text{ or } CH_3{+}SH}, \quad (3.3)$$

exhibits broad maxima (Vaghjiani, 1993) at ~205 nm and between 227 nm (Mouflih *et al.*, 1988) and 230 nm (Vaghjiani, 1993). The two lowest electronically excited states of methyl mercaptan, the $1^1A''$ and $2^1A''$ states (C_s point-group symmetry is assumed throughout this discussion), are responsible for this absorption; see Fig. 10. It has been shown that these two potential-energy surfaces exhibit a surface of conical intersection (Yarkony, 1994).

This subsection studies this surface of conical intersection and considers its implications for the reaction (3.3). Ideally this reaction should be treated in the full 12-dimensional internal coordinate space. This is not practical, even using the most modern computational tools, and so a reduced dimensionality approach is sought. The simplest approach consistent with reaction (3.3) is a two-dimensional model involving the CS and SH bond distances, $R(\mathrm{CS})$ and $R(\mathrm{SH})$. The adiabatic predissociation on the $1^1A''$ potential-energy surface has been studied in this way (Stevens *et al.*, 1995). According to the noncrossing rule, this space of dimension 2 should have, at most, isolated points of conical intersection. Thus the focus of this subsection is a single representative point on the surface of conical intersection in the Franck-Condon region of reaction (3.3). The point of conical

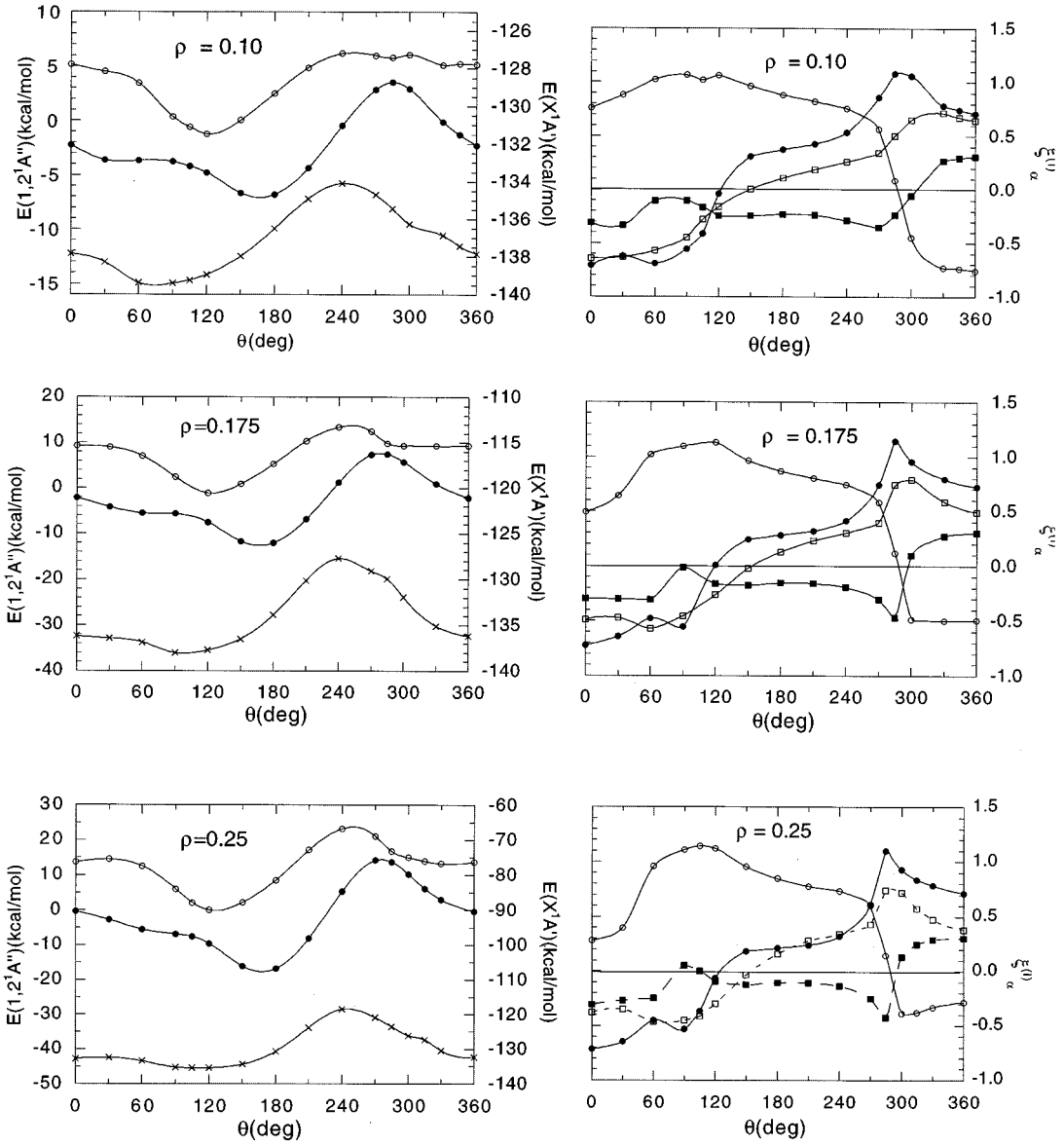

FIG. 12. CH_3SH: Left plates: E_I, $I=1,2^1A''$ left-hand ordinate and $E_{1^1A'}$ right-hand ordinate, as a function of θ for fixed ρ. Right plates: $\bar{\chi}_\alpha^I$ as a function of θ for fixed ρ: ○, ●, Rydberg s orbital on sulfur; □, ■ diffuse s orbital on carbon. Bottom row ρ=0.25, middle row ρ=0.175, and top row ρ=0.10. Filled markers denote the $1^1A''$ state, and open markers denote the R^1A'' state.

intersection was obtained from the solution of Eq. (2.19) with the constraint $R(\mathrm{CS})=3.58a_0$. At this point of conical intersection, $\mathbf{R}_x$, the following values obtain—each compared with the corresponding value predicted for $\mathbf{R}_{\mathrm{eq}}$ the equilibrium geometry of X^1A' state, shown in parentheses: $R(\mathrm{CS})=3.580(3.495)a_0$, $R(\mathrm{SH})=2.406(2.536)a_0$, $R(\mathrm{CH}^1)=2.076(2.048)a_0$, $R(\mathrm{CH}^2)=2.073(2.045)a_0$, and $\angle\mathrm{CSH}=101.4°(96.3°)$. As discussed elsewhere, the computed parameters for $\mathbf{R}_{\mathrm{eq}}$ differ only slightly from geometrical parameters deduced from microwave spectroscopy (Kojima and Nishikawa, 1957). Thus $\mathbf{R}_x$ differs from $\mathbf{R}_{\mathrm{eq}}$ principally in the CS and SH bond distances, which are stretched and compressed by $0.085a_0$ and $0.13a_0$, respectively. At $\mathbf{R}_x$ the $1,2^1A''$ states are degenerate to 0.4 cm^{-1} [a measure of the precision of the algorithm based on Eq. (2.19)], and the common energy is $E_{1^1A''}=E_{2^1A''}=50420$ cm^{-1} measured relative to $E_{X^1A'}(\mathbf{R}_{\mathrm{eq}})$.

$\mathbf{R}_x$ was chosen as representative because of the proximity of the coordinates other than $R(\mathrm{CS})$ and $R(\mathrm{SH})$ to their values at $\mathbf{R}_{\mathrm{eq}}$. The constraint $R(\mathrm{CS})=3.58a_0$ was designed to keep the conical intersection in the Franck-Condon region to the extent possible while retaining a reasonable excitation energy. These attributes are also desirable for treating nonadiabatic photodissociation originating on the $2^1A''$ potential-energy surface, since a recent study of conical intersections in hydroxylamine (Hettema and Yarkony, 1995; see Sec. III.D) indicates that it is the energetically accessible conical intersections in the vicinity of the initially excited wave packet, rather

than the lowest-energy conical intersections, that are involved in the photodissociation process.

2. The g-h plane: Berry phase and energetics

The g-$h(\mathbf{R}_x)$ plane, constructed as discussed in Sec. II, is pictured on the center plates in Fig. 11. Here it is important to recall that the individual $\mathbf{g}^{IJ}$ and $\mathbf{h}^{IJ}$ directions are quite arbitrary, whereas the g-h plane is well defined. This point was checked numerically by determining $\mathbf{g}^{IJ}$, $\mathbf{h}^{IJ}$ and the g-h plane for the last two iterations in the solution of Eq. (2.19). $\mathbf{g}^{IJ}$ and $\mathbf{h}^{IJ}$ changed dramatically, while the g-h plane was virtually unchanged. Circular g-h paths will be defined in terms of polar coordinates $x=\rho\cos\theta$, $y=\rho\cos\theta$ where unit vectors $\hat{x}$ (predominantly C-S stretch) and $\hat{y}$ (predominantly S-H stretch) are defined by $\hat{x}=\mathbf{h}^{IJ}/\|\mathbf{h}^{IJ}\|$ and $\hat{y}=\bar{\mathbf{g}}^{IJ}/\|\bar{\mathbf{g}}^{IJ}\|$ and $\bar{\mathbf{g}}^{IJ}\equiv\mathbf{g}^{IJ}-(\mathbf{g}^{IJ\dagger}\cdot\hat{x})\hat{x}$. For reasons discussed below only g-h paths with $\rho\leqslant 0.25a_0$ are considered.

In Fig. 11 the geometrical changes associated with a circular g-h path around $\mathbf{R}_x$ are presented. R(CS), R(SH), and $\angle$CSH are indicated explicitly for ρ=0.10, 0.175, $0.25a_0$, and the indicated values of θ, although in the figure ρ=1.0 is used to emphasize the structural changes. The internuclear distances not explicitly reported in Fig. 11 exhibit smaller deviations from their values at $\mathbf{R}_x$. Along a circular g-h path with ρ=0.25, $R(\mathrm{CH}^i)$, where i=1–3, changes by less than $0.1a_0$, while $\angle\mathrm{H}^1\mathrm{CS}$ changes by less than $\pm 2°$.

The principal geometrical changes along a g-h path reflect the phase relationships between $\cos\theta$ and $\sin\theta$ and the character of the $\mathbf{h}^{IJ}$ and $\bar{\mathbf{g}}^{IJ}$ axes noted above. Defining $\delta(Z)\equiv R(Z)-R_x(Z)$, we find that the extreme values of δ(CS) occur near θ=0° and 180°, while those for δ(SH) occur near θ=90° and 270°. The first quadrant corresponds to decreased δ(CS) and increased δ(SH), while the third quadrant corresponds to decreased δ(SH) and increased δ(CS). In the second quadrant both the SH and CS bonds are stretched, while in the fourth quadrant both the SH and CS bonds are compressed. Thus the g-h path can lead to either of the two channels described in reaction (3.3). From Fig. 11 it can be seen that nuclear configurations in the first quadrant explore the Franck-Condon region of reaction (3.3).

The g-h plane characterizes nuclear motions that produce the Berry phase effect. However, as noted in Sec. II, it is necessary to confirm the existence of the sign change for each ρ considered. It is also important to determine the energetics along these paths, since it is these energetics rather than the energy of the conical intersection itself that determine whether the geometric phase effect will affect the nuclear dynamics. These issues are addressed in Fig. 12. The left-hand column in Fig. 12 reports the energy for ρ=0.10, 0.175, and 0.25, while the right-hand column addresses the question of the phase behavior along these closed loops.

For technical reasons the demonstration of the geometric phase effect is not entirely straightforward for the class of wave functions used to characterize this system. Near $\mathbf{R}_x$ the $\tilde{X}^1A'$, $1,2^1A''$ electronic states are described by the following electron configurations:

$$[1a'^2\cdots 7a'^2 \quad 1a''^2 2a''^2] \quad 8a'^2 9a'^2 10a'^2 3a''^2, \ \tilde{X}^1A', \tag{3.4a}$$

$$[1a'^2\cdots 7a'^2 \quad 1a''^2 2a''^2] \quad 8a'^2 9a'^2 10a'^2 3a''\xi^{(1)}, \ 1^1A'', \tag{3.4b}$$

$$[1a'^2\cdots 7a'^2 \quad 1a''^2 2a''^2] \quad 8a'^2 9a'^2 10a'^2 3a''\xi^{(2)}, \ 2^1A''. \tag{3.4c}$$

Since the principal change in the character of the $1,2^1A''$ wave functions involves mixing of $\xi^{(1)}$ and $\xi^{(2)}$ (symmetry designations $11a'$ and $12a'$), a simple diagnostic for the phase of the wave functions can be constructed. As discussed elsewhere, it is possible to define composite molecular orbitals $\bar{\xi}^{(1)}$ and $\bar{\xi}^{(2)}$ whose phase behavior mimics that of $\Psi_{1^1A''}$ and $\Psi_{2^1A''}$, respectively. The reader interested in the details of this construction should consult Yarkony (1996c). The right-hand column in Fig. 12 reports representative components of $\bar{\xi}^{(I)}$, I=1,2. The geometric phase effect is present for each ρ considered, since $\bar{\xi}^{(I)}(\rho,0°)=-\bar{\xi}^{(I)}(\rho,360°)$, so that real-valued wave functions that are continuous with respect to θ are not single-valued functions of θ.

The energetic data in Fig. 12 evince minima in $E_{2^1A''}-E_{1^1A''}$ near θ=285°. Relative to the energy at the conical intersection, an additional 15, 9, and 4 kcal/mol are required for ρ=0.25,0.175,$0.10a_0$ to circumnavigate the conical intersection on the $1^1A''$ potential-energy surface. This additional barrier to circumnavigating the conical intersection occurs near θ=285° as a result of the compression of the SH bond.

3. Relation to photodissociation

The ultraviolet absorption of methyl mercaptan in the range ~193–240 nm is the focus of the present discussion. The long-wavelength end of this absorption involves only the $1^1A''$ electronic state, while the short-wavelength end can involve either or both of the $1,2^1A''$ states. It is desirable, then, to treat the long-wavelength absorption using a single adiabatic surface, while for shorter wavelengths two potential-energy surfaces are required. At $\mathbf{R}_x$, $E_{1^1A''}(\mathbf{R}_x)=E_{2^1A''}(\mathbf{R}_x)=50420$ cm^{-1}, only 990 cm^{-1} greater than $E_{2^1A''}(\mathbf{R}_{\mathrm{eq}})$, so that this conical intersection is predicted to be energetically accessible with 193 nm light used in recent experimental studies (Jensen *et al.*, 1993) of reaction (3.3) but not with the 230 nm photons corresponding to the first absorption maximum. However, as noted in the Introduction, accurate single-surface dynamics must consider the possibility of a geometric phase effect induced by an energetically remote conical intersection.

The energetics in the g-$h(\mathbf{R}_x)$ plane discussed in the previous subsection can be used to consider this possibility in (the two-dimensional description of) the photodissociation dynamics restricted to the $1^1A''$ potential-energy surface. Key here is the portion of the closed loop near θ=285°, which provides a barrier to circumnavigating the conical intersection. The height of this barrier increases with increasing ρ. Thus energetically accessible paths are expected to pass quite close to the conical intersection point itself, which from the above discussion is at approximately 198 nm. This energy is higher than the maximum, but within the breadth of the second (stronger) absorption band, 193–210 nm (Vaghjiani, 1993), of CH_3SH.

Thus it is unlikely that the adiabatic $1^1A''$-state dynamics will be influenced by the geometric phase effect. However, at shorter wavelengths, for which the $2^1A''$ potential-energy surface is involved in the excitation process, the conical intersections discussed here and previously (Yarkony, 1994) are essential for rapid photodissociation. In this case derivative coupling data, such as those presented elsewhere (Yarkony, 1996c), are required for the quantitative treatment of photodissociation dynamics. Wave packets dissociating from the $2^1A''$ potential-energy surface via the conical intersection will span the entire range of θ for a given ρ, since ρ will be small. Thus incorporation of the geometric phase effect into a formulation of the dynamics using two adiabatic states is essential.

The g-$h(\mathbf{R}_x)$ plane cannot be used without suitable modification to develop a two-dimensional model of the photodissociation process. In the vicinity of $\mathbf{R}_x$, that is, for the range of ρ considered here, motion in the g-$h(\mathbf{R}_x)$ plane involves principally changes in R(CS) and R(SH). However, as ρ increases, significant distortions of the CH_3 moiety are observed. The g-$h(\mathbf{R}_x)$ plane would have to be distorted to limit changes in the CH_3 moiety as ρ increases. In this regard it should be noted the g-h plane is not unique in displaying the Berry phase effect. Any closed loop obtained by continuously distorting a closed loop in the g-h plane (which includes an odd number of points of conical intersection) will display the Berry phase effect. The (ρ,θ) coordinate system suggested in this work, suitably modified to limit changes in the CH_3 moiety, would permit incorporation of the geometric phase effect into an adiabatic-state treatment of the nuclear dynamics.

C. Comments on closed loops surrounding a point of conical intersection

It is useful at this point to consider in more detail the g-h paths (and associated energetics) for CH_2 and CH_3SH presented in Figs. 7 (9) and 11 (12), respectively, and to compare them with the g-h path in H_3, a path uniquely determined by symmetry. The g-h path for H_3 is given by (Herzberg and Longuet-Higgins, 1963) $H^1 + H^2H^3(\theta = 0) \rightarrow H^1H^2H^3(\theta = 60) \rightarrow H^1H^2 + H^3(\theta$=120) $\rightarrow H^1\,H^2\,H^3(\theta = 180) \rightarrow H^1\,H^3 + H^2(\theta = 240) \rightarrow H^1\,H^2H^3$ (θ=300) $\rightarrow H^1 + H^2H^3(\theta$=360). Thus along this path there is an exchange of hydrogens between the long-bond (H^1 with H^2H^3 at θ=0°) and short-bond (H^2 with H^3 at θ=0°) configurations. This exchange is achieved by passing through structures in which the three atoms are in close proximity. In this case it can be shown (Yarkony, 1996) that, taking the origin as the minimum energy point on the seam of conical intersections, for $\rho \leqslant 0.75$ the energy of the lower adiabatic potential energy surface along the g-h path is *uniformly less* than energy at the conical intersection.

Along the g-h path for CH_2 the molecular configurations are given by HC+H(θ=90°) $\rightarrow CH_2(\theta$=180°) $\rightarrow$H+CH(θ=270°) $\rightarrow CH_2(\theta$=360°). As in H_3 the long- and short-bond configurations are separated by more intimately interacting configurations. This exchange of bonding hydrogens along the g-h path explains why the geometric phase effect in the H_2+H, and the CH+H, reactions is associated with H exchange. In CH_2 this H exchange originates from the $\mathbf{h}^{IJ}$ displacement. From Fig. 9 it is seen that it is displacements along this coordinate (θ=90°, 270°) that produce a local barrier barrier on the lower adiabatic potential energy surface along the g-h path. Note however that, as in $H+H_2$, the energy at the barrier is lower than the energy at the conical intersection itself. The height of the barrier is key since it determines the energy at which the geometric phase effect will influence the dynamics.

Along the g-h path for CH_3SH the molecular configurations are given by $CH_3S+H(Q1) \rightarrow CH_3+S+H(Q2)$ $\rightarrow CH_3+SH(Q3) \rightarrow CH_3SH(Q4)$, where QI indicates that θ is in the Ith quadrant. As in H_3 and CH_2, there is a change in bonding, SH (in Q3) $\leftrightarrow$ CS (in Q1), in between which the CS and SH bonds are either both stretched or both compressed. As in CH_2 it is a bond-stretched–bond-compressed configuration that produces a barrier along the path on the lower adiabatic potential energy surface. However here the energy at the barrier is higher than the energy at the conical intersection. In a sense then the situation in methyl mercaptan is similar to that in the triatomic molecules, CH_2 and H_3. However, the triatomic analogy is simplistic since, as the discussion in Sec. III.B points out, the CH_3 moiety is not a spectator but undergoes changes in character that become evident as ρ increases.

While in each case the g-h paths have qualitative similarities, the details of the energetics along the paths differ. The key quantitative difference—the height of the barrier—represents the interplay between the energetics of bond stretching and bond compression and must be determined on a case-by-case basis.

D. Multistate processes induced by conical intersections in general polyatomic systems: The case of hydroxylamine

1. Introduction

Hydroxylamine (NH_2OH) is a particularly interesting example for the study of the effects of conical intersections in photodissociation. NH_2OH can be viewed as a derivative of ammonia, H-$NH_2 \rightarrow$HO-NH_2, a classic sys-

tem in the field of (nonadiabatic) photodissociation (McCarthy *et al.*, 1987), and has recently been the subject of laboratory studies. It has a weak N-O bond that can be broken photochemically, as evidenced by recent, direct, and vibrationally mediated photodissociation studies (Crim, 1993; Scott, 1994). The photodissociation of hydroxylamine is considered here as an example of the complexities of a photodissociation process and the ways in which Eq. (2.19) can be used to deal with these complexities.

The ground state of hydroxylamine has C_s symmetry (see Fig. 13), so it is natural to label the relevant electronically excited states using this symmetry designation. The principal electron configurations of the electronic states considered, at the equilibrium geometry of the $X^1A' \equiv 1^1A'$ state, are

$$1^1A': \quad 1a'^2\cdots 5a'^2 1a''^2 6a'^2 7a'^2 2a''^2, \tag{3.5a}$$

$$2^1A': \quad 1a'^2\cdots 5a'^2 1a''^2 6a'^2 7a' 8a' 2a''^2, \quad 7a' \rightarrow 8a', \tag{3.5b}$$

$$3^1A': \quad 1a'^2\cdots 5a'^2 1a''^2 6a'^2 7a' 9a' 2a''^2, \quad 7a' \rightarrow 9a', \tag{3.5c}$$

$$1^1A'': \quad 1a'^2\cdots 5a'^2 1a''^2 6a'^2 7a'^2 8a' 2a'', \quad 2a'' \rightarrow 8a', \tag{3.5d}$$

$$2^1A'': \quad 1a'^2\cdots 5a'^2 1a''^2 6a'^2 7a'^2 9a' 2a'', \quad 2a'' \rightarrow 9a', \tag{3.5e}$$

Also indicated above are the excitation levels for the four excited states, relative to the $1^1A'$ state. In a qualitative sense the $7a', 2a''$ orbitals represent nitrogen and oxygen lone pairs, while the $8a', 9a'$ represent N-O antibonding. Rydberg orbitals, respectively. Thus the photodissociation processes to be considered are

$$NH_2OH(X^1A') + h\nu \rightarrow NH_2OH(2,3^1A',1,2^1A'') \rightarrow NH_2OH(1^1A',1^1A'') \rightarrow OH(X^2\Pi) + NH_2(\tilde{X}^2B_1), \quad \Delta E \sim 18.0 \text{ eV}, \tag{3.6a}$$

$$NH_2OH(X^1A') + h\nu \rightarrow NH_2OH(2,3^1A',1,2^1A'') \rightarrow NH_2OH(2^1A',2^1A'') \rightarrow OH(X^2\Pi) + NH_2(\tilde{A}^2A_1), \quad \Delta E \sim 19.3 \text{ eV}, \tag{3.6b}$$

where ΔE reflects only the N-O bond energy noted above and T_e=10291 cm^{-1} (Herzberg, 1966) for the $\tilde{A}^2A_1$ excited state of NH_2. Figure 13 presents a schematic, and, as shown below, somewhat simplistic, picture of this photodissociation.

The C_s regions of the potential-energy surfaces must be considered, since they will be the regions of nuclear coordinate space initially probed by the photoexcitation process. This restriction is also important from a conceptual perspective. It eliminates the possibility of characterizing as "same-symmetry" intersections, intersections of states that correlate with distinct symmetry ($^1A'$ and $^1A''$) states for C_s geometries and that have been "insignificantly" changed by nuclear motions that remove the C_s symmetry.

As a first step in this regard, Fig. 14 reports $E_{i^1A'}$, i=1–3 and $E_{i^1A'}$, i=1,2 as a function of R(N-O) with the remaining geometrical parameters constrained to their values in the ground-state equilibrium structure. However, the constraint of C_s symmetry does preclude consideration of internal rotation around the N-O bond and must be relaxed. This point is addressed in Fig. 15, which reports E_{i^1A}, i=1–5 as a function of κ, the torsional angle between the H^1O and the H^2H^3 lines projected onto the plane perpendicular to the N-O axis (see Fig. 13). The C_s symmetry structure in Fig. 13 corresponds to κ=90°. For $\kappa \neq 90°$ the 2^1A state can readily be identified as a perturbed $2^1A'$ state. However, the $3^1A'$ and $1^1A''$ states, nearly degenerate for κ=90°, are strongly mixed as κ decreases. This point will be discussed further below. From Fig. 15 it can be seen that E_{2^1A} and E_{3^1A} are increasing functions of κ for $0<\kappa<90°$ with minimal values at κ=0°, while E_{4^1A} increases as κ decreases from κ=90°.

2. Conical intersections and energetics

In the discussions that follow it will be convenient to define $\delta R(XY) \equiv R(XY) - R_{eq}(XY)$ and $\tilde{\angle} XYZ \equiv \angle XYZ - \angle_{eq} XYZ$ where the equilibrium distances and angles for the X^1A' state will be denoted $R_{eq}(XY)$ and $\angle_{eq} XYZ$; see caption to Fig. 13. Conical intersections will be sought in which R(NO) is fixed at values close to its value for the X^1A'-state equilibrium geometry, R_{eq}(NO), and the remaining geometrical parameters are determined to minimize the energy of the point on the surface of conical intersection.

a. Surfaces of conical intersection: C_s symmetry

The potential for conical intersections can be seen from Fig. 14. Near δR(NO)=0 the $1^1A''$ and $3^1A'$ states are nearly degenerate, separated by less than 450 cm^{-1}. An avoided intersection of the $2^1A'$ and $3^1A'$ states, and a symmetry-allowed accidental degeneracy of the $1^1A''$

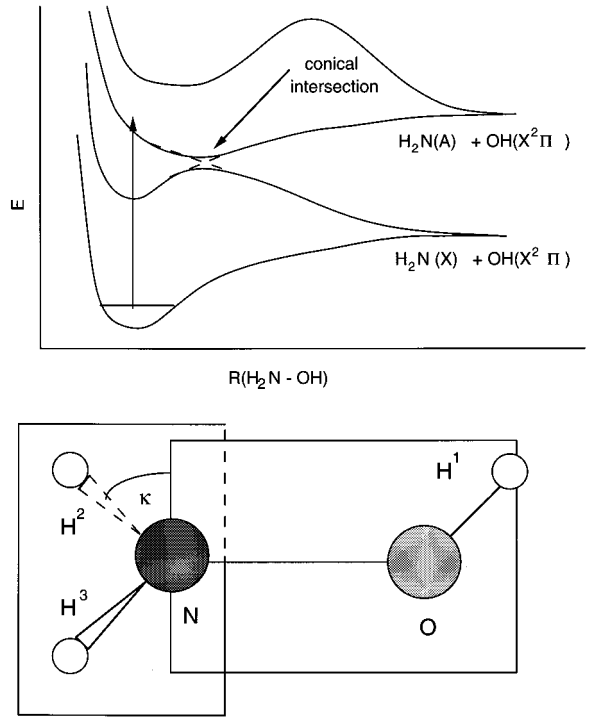

FIG. 13. NH_2OH: Schematic representation of photodissociation process and geometrical arrangement at the equilibrium geometry, $Rr_{eq}(OH^1) = 1.7865(1.818 \pm 0.015)$, $R_{eq}(NO) = 2.7686(2.746 \pm 0.004)$, $R_{eq}(NH^2) = 1.8917(1.920 \pm 0.009)$, $\angle_{eq}H^1ON = 102.17(101.4 \pm 0.5)$, $\angle_{eq}ONH^2 = 103.62$ (103.2 ± 0.5), $\angle_{eq}H^2NH^3 = 106.87(107.1 \pm 0.5)$, of the $1^1A'$ state of hydrox ylamine. Experimental values from Tsunekawa (1972) given parenthetically.

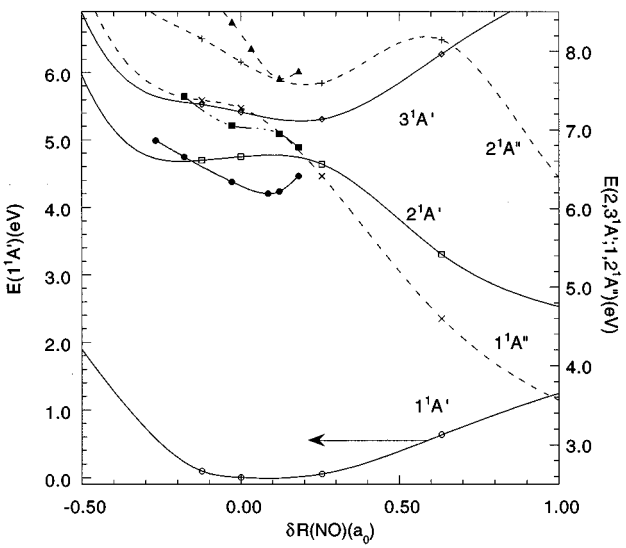

FIG. 14. NH_2OH: $R(NO)$ dependence of $E_{i^1A'}(eV)$, i=1–3 and $E_{i^1A''}(eV)$, i=1,2. All other geometrical variables fixed at equilibrium values for $1^1A'$ state. Points on the surfaces of intersection: ●, $2^1A'$-$3^1A'$; ▲, $1^1A''$-$2^1A''$; ■, $2^1A'$-$1^1A''$.

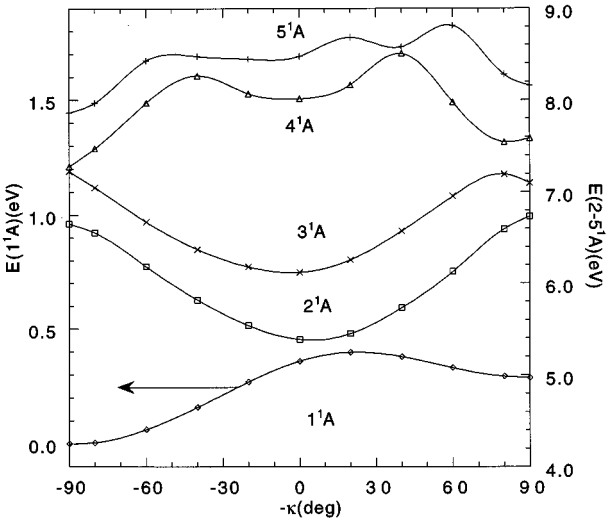

FIG. 15. NH_2OH: κ dependence of $E_{i^1A}(eV)$, i=1–5. All other geometrical variables fixed at equilibrium values for $1^1A'$ state.

and $2^1A'$ states, is evident for $\delta R(NO) \sim 0.24a_0$. An avoided intersection of the $1^1A''$-$2^1A''$ states is evident near $\delta R(NO) = 0.04a_0$. The points on the surfaces of conical intersection are reported in Table I and in Fig. 14.

The surface of conical intersection with the lowest energy, for the geometrical range considered in this study, is the $2^1A'$-$3^1A'$ surface of intersection. From Table I it can be seen that as a function of $R(NO)$, $\delta R(OH)$ and $\delta R(NH^2)$ vary little, while the angles $\angle H^1ON$, $\angle H^2NH^3$, and $\angle ONH^2$ exhibit considerable variation. The minimum-energy point on the $2^1A'$-$3^1A'$ surface of conical intersection, $\mathbf{R}_{mex}(2^1A'\text{-}3^1A')$, occurs at $R(NO) = 2.8539a_0$ and $R(OH^1) = 1.9325a_0$ with $E_{2^1A'} = E_{3^1A'} = 6.19$ eV. From Fig. 14 it can be seen that this and several other points on this surface of intersection have energy less than $E_{2^1A'}$ for the corresponding value of $R(NO)$ with the remaining coordinates fixed at their $\mathbf{R}_{eq}$ values. This reflects the "relaxation" of the remaining internal coordinates and has been observed in previous treatments of conical intersections in CH_3SH (Yarkony, 1994) and CH_3SCH_3 (Manaa and Yarkony, 1994). These observations demonstrate that models of NH_2OH nonadiabatic photodissociation that neglect changes in coordinates other than $R(NO)$ are likely to be unsuccessful in characterizing this process.

The $1^1A''$-$2^1A''$ surface of intersection presented in Table I and Fig. 14 is considerably higher in energy than the $2^1A'$-$3^1A'$ surface of intersection. In this case $\mathbf{R}_{mex}(1^1A''\text{-}2^1A'')$ lies above the corresponding $E(2^1A'')$. For this reason the $1^1A''$-$2^1A''$ surface of conical intersection will not be considered further.

Also considered in Table I are the $2^1A'$-$1^1A''$ and $3^1A'$-$1^1A''$ symmetry-allowed surfaces of intersection. As noted in Sec. II, these intersections are conical when nontotally symmetric C_s internal modes are considered. For three points on the $2^1A'$-$1^1A''$ surface of intersection both $R(NO)$ and $R(OH^1)$ were fixed, with

TABLE I. Points on the C_s section of the I-J surface of conical intersections. Bond lengths $R(AB)$ are in atomic units (a_0=0.0529 nm). Angles are in degrees, the energy $E_x=E_I=E_J$ is in eV, and the energy splitting $\Delta E_{IJ}\equiv E_I-E_J$ is in cm^{-1}. R(NO) is fixed and all the other parameters are optimized except as noted.

R(NO)	R(OH^1)	R(NH^2)	∠H^{1}ON	∠ONH^2	∠H^{2}NH^3	E_x	ΔE_{IJ}
			$2^1A'$-$3^1A'$ surface of intersection				
2.50	1.9750	2.0167	133.5	124.3	105.9	6.86	0.39
2.59	1.9738	1.9805	128.9	124.1	108.3	6.65	0.73
2.74	1.9518	1.9213	117.8	122.8	113.7	6.33	0.11
2.853912[a]	1.9325	1.8841	105.7	118.3	123.4	6.17	0.04
2.89	1.9320	1.8861	102.2	115.3	129.0	6.21	1.44
2.95	1.9024	1.9475	99.4	107.6	144.8	6.41	0.15
			$1^1A''$-$2^1A''$ surface of intersection				
2.59	1.8663	2.1661	117.7	116.4	78.1	8.91	0.09
2.74	1.7661	2.0976	105.7	116.8	91.2	8.37	0.11
2.80	1.7594	2.0285	93.8	114.7	96.4	8.03	0.13
2.89	1.8526	2.0585	85.0	104.7	97.1	7.65	0.18
2.95	2.0930	2.0281	74.2	104.7	100.7	7.75	2.96
			$2^1A'$-$1^1A''$ surface of intersection				
2.59	1.96[b]	1.9008	118.7	102.5	106.2	7.42	1.91
2.74	1.96[b]	1.9122	109.5	98.5	103.9	7.05	0.56
2.89	1.96[b]	1.9031	106.8	99.9	110.3	6.95	0.02
2.95	1.8737	1.8960	113.3	102.7	109.8	6.78	0.00
			$3^1A'$-$1^1A''$ surface of intersection				
2.59	2.1448	1.9062	111.6	108.2	112.3	7.16	0.48
2.74	2.0667	1.9050	111.7	105.8	112.2	7.06	1.39
2.89	1.9502	1.9043	114.1	102.8	110.3	6.95	0.60
2.95	1.8711	1.9033	109.2	103.9	112.0	6.83	0.24

[a] R(NO) was also optimized in this calculation.
[b] R(OH^1) fixed in this calculation.

R(OH^1)=1.96a_0, that is, near its value on the $2^1A'$-$3^1A'$ surface of intersection, to avoid regions of nuclear coordinate space for which δR(OH^1) is large. At shorter values of R(OH^1), solutions to Eq. (2.19) were not found.

For the points reported on the $2^1A'$-$3^1A'$ surface of intersection, $E_{2^1A'}=E_{3^1A'}<E_{1^1A''}$, whereas for points reported on the $2^1A'$-$1^1A''$ surface of intersection, $E_{2^1A'}=E_{1^1A''}<E_{3^1A'}$. Interestingly, then, both the $2^1A'$-$1^1A''$ and $2^1A'$-$3^1A'$ surfaces of intersection correspond to intersections of the second and third electronic states of hydroxylamine. The mixing of $3^1A'$ and $1^1A''$ states that is responsible for this has important consequences and is discussed further below.

b. Surfaces of conical intersection: No spatial symmetry

Figure 15 suggests that the lowest-energy-points on the 2^1A-3^1A surface of conical intersection will occur for non-C_s geometries. Table II reports points on the surface of conical intersections of the 2^1A and 3^1A states for $\kappa\neq 90°$. Comparing the portions of $2^1A'$-$3^1A'$ and 2^1A-3^1A surfaces of intersection reported in Tables I and II, the latter occur at energies lower by approximately 0.75 eV, smaller values of δR(OH^1)—that is, closer to δR(OH^1)=0—and values of κ rotated nearly 90° degrees.

3. Photodissociation: Mechanistic considerations

The 3^1A state correlates adiabatically with the product channel of process (3.6b), the production of $NH_2(\tilde{A}^2A_1)$, but can produce ground-state products by accessing the 2^1A-3^1A surface of conical intersection. Characterization of photofragments resulting from the initial excitation of the 3^1A state requires a treatment of the nuclear dynamics, which is beyond the scope of the present review. However, important mechanistic insights can be gained by following the steepest-descent path from a reference geometry, here taken as either (i) the equilibrium geometry of the X^1A' state with κ changed from 90° to 88°, $E_{3^1A}\sim 7.22$ eV (see Fig. 14), or (ii) the equilibrium geometry with κ changed from 90° to 0°, $E_{3^1A}=6.14$ eV (see Fig. 15). These points were chosen to illustrate the range of nuclear coordinates accessible

TABLE II. Points on the 2^1A-3^1A surface of conical intersection. Distances are in a_0, angles are in degrees, the energy $E_x = E_I = E_J$ is in eV, and the energy splitting $\Delta E_{IJ} \equiv E_I - E_J$ is in cm^{-1}. R(NO) is fixed and all the other parameters are optimized except as noted.

R(NO)	R(OH^1)	R(NH^2) R(NH^3)	$\angle$H^{1}ON	$\angle$ONH^2 $\angle$ONH^3	$\angle$H^{2}NH^3	κ	E_x	ΔE_{IJ}
			Energy minimized points					
2.6686	1.8863	1.9928	118.3	138.2	105.6	8.42	5.64	0.32
		1.9237		116.3				
2.7686	1.8524	1.9474	110.7	132.2	114.4	9.61	5.43	0.13
		1.9060		113.5				
2.8145[a]	1.8431	1.9371	107.2	128.0	120.0	12.3	5.38	0.25
		1.9044		112.0				
2.89	1.8423	1.9515	101.0	119.7	130.9	10.1	5.42	0.14
		1.9102		109.4				
δR(NO) [R(NO)]	δR(OH^1) [R(OH^1)]	δR(NH^2) δR(NH^3)	$\tilde{\angle}$H^{1}ON	$\tilde{\angle}$ONH^2 $\tilde{\angle}$ONH^3	$\tilde{\angle}$H^{2}NH^3	κ	δE[d]	ΔE_{IJ}
			Near steepest-descent points					
0.0639	0.1405	0.0298	9.03	12.08	10.93	81.3	–0.86	1.63[b]
[2.8325]	[1.9270]	0.0259		8.58				
0.1534	0.0227	0.0529	–1.77	4.580	4.63	1.53	–0.38	0.35[c]
[2.9222]	[1.8092]	0.0445		3.280				

[a] R(NO) was also optimized in this calculation.

[b] Steepest descent begun from X^1A' equilibrium structure except that $\kappa \to 88°$.

[c] Steepest descent begun from X^1A' equilibrium structure except that $\kappa \to 0°$.

[d] $\delta E = E_{3^1A}(\mathbf{R}_x) - E_{3^1A}(\mathbf{R}_{\text{ref}})$ where $\mathbf{R}_{\text{ref}}$ is the equilibrium geometry of the X^1A' state with κ modified as indicated and $\mathbf{R}_x$ is the point on the surface of conical intersection.

in the photodissociation process. They will be referred to as the high- and low-energy excitation regions, respectively. In an adiabatic process, these paths would lead to a metastable structure, a local minimum of the 3^1A surface, or dissociated fragments. However, here it was found that in each case the steepest-descent path approached the 2^1A-3^1A surface of intersection. When the steepest-descent path on a surface approaches a conical intersection point, the steepest-descent algorithm will begin to oscillate (see Fig. 16), unless a very small step size is used. This oscillation is a signature of a conical intersection. From the point where the oscillation begins, the steepest-descent path could be followed to the conical intersection with a very small step size. However, it is more efficient to locate approximately the conical intersection point on the steepest-descent path using Eq. (2.19), starting from the point where oscillation begins and heavily damping the portion of the hessian Q^{IJ} corresponding to energy minimization, as discussed in Sec. II. The results of this procedure are presented in the second part of Table II. Note that, for the path originating at $\kappa \sim 90°$, $\delta R(\text{OH}^1) \sim 0.15a_0$ while δR(NO) is small (consistent with the results in Table I). For the path originating at $\kappa = 0°$ the opposite is true, $\delta R(\text{OH}^1)$ is small while $\delta R(\text{NO}) \sim 0.15a_0$.

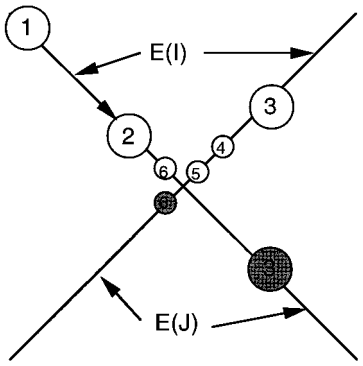

FIG. 16. NH_2OH: Steepest-descent path on surface I in the vicinity of conical intersection of states I and J. Points on computed steepest-descent path, open circles, illustrate oscillation of steepest-descent algorithm with finite step size as algorithm attempts to move to filled circle points on surface J.

This steepest-descent analysis shows that, following excitation to the 3^1A surface, either in the center of the Franck-Condon region $\kappa \sim 90°$ or in its low-energy tail $\kappa \sim 0°$, the system is likely to behave nonadiabatically, encountering a conical intersection of the 2^1A and 3^1A states that will lead to ground-state products. It is important to note that, while the energy of a point on a surface of conical intersection determines whether it is accessible, only an analysis of the nuclear motion on the surface in question can determine whether that conical intersection region is accessed. In particular, note that the nuclear dynamics, following excitation to the 3^1A state in the high-energy $\kappa \sim 90°$ portion of the Franck-Condon

region, is not likely to sample the minimum-energy region of the 2^1A-3^1A surface of conical intersection that occurs for $\kappa \sim 10°$, but rather the geometrically closer region indicated in row 5 of Table II. Similarly the steepest-descent path originating at $\kappa = 0°$ encounters the region of the 2^1A-3^1A surface of conical intersection that is 0.35 eV above the minimum-energy crossing point (see rows 3 and 6 in Table II).

IV. CONCLUSIONS AND IMPLICATIONS

Conical intersections of two states of the same symmetry can have important implications both for explicitly nonadiabatic processes, that is, processes in which the nuclear dynamics takes place on more than one Born-Oppenheimer potential-energy surface, and for adiabatic, single-potential-energy-surface processes. Of particular concern here was the ''diabolical'' nature of this class of conical intersections, which was attributed to the difficulty in (i) anticipating the existence of the conical intersection itself and (ii) determining the pathways that may give rise to the geometric phase effect. Despite the inherent difficulty in anticipating their existence, it is suggested that when one is concerned with electronically excited states these conical intersections should not be viewed as rare occurrences.

This issue is of more than academic interest. Advances in laser design have led to proposals for control of chemical reactions using electronically excited states as ''intermediates.'' In such situations the geometric phase effect may be encountered. It has been suggested, for example, that control of a chemical reaction may be achieved by using tailored pulses in pump-dump experiments (Tannor and Rice, 1985, 1988; Tannor *et al.*, 1986). In these processes the system propagates for a time on an electronically excited potential-energy surface before being dumped back onto the ground-state surface. If the excited state exhibits a conical intersection, proper treatment of the geometric phase effect will be required to correctly predict the outcome of these experiments. In this regard note that very recent dynamics studies of model Jahn-Teller systems have demonstrated that the geometric phase effect can have a significant impact on femtosecond pump-probe experiments (Schön and Köppel, 1994, 1995).

In a related vein it has been proposed (Romero-Rochín and Cina, 1989; Cina and Romero-Rochin, 1990; Cina, 1991; Cina *et al.*, 1993) that the geometric phase effect can be observed in molecules ''directly,'' that is without elaborate spectral fitting, in very sophisticated spectroscopically based experiments using ultrafast laser pulses (Scherer *et al.*, 1990, 1992). Such a direct observation would provide a striking example of the geometric phase effect.

The geometric phase effect was originally discovered in a particular, somewhat rare, class of molecular systems, those that exhibit a dynamic Jahn-Teller effect (Longuet-Higgins *et al.*, 1958). However, as a result of the seminal work of Berry (1984), the implications of this effect have been sought principally outside the area of molecular spectroscopy. The issues raised in this review suggest that the time has come to revisit the role of this most diabolical phenomenon in chemical processes.

ACKNOWLEDGMENTS

The author wishes to thank L. Butler, J. Cina, B. Kendrick, A. Kupperman, C. A. Mead, and M. Robb for providing preprints/reprints of their work. The author gratefully acknowledges the hospitality of M. van Hemert of the Gorleaus Laboratory in Leiden, The Netherlands and G. Parlant of the LCPR in Orsay, France, where significant portions of this manuscript were prepared. This work was supported in part by DOE-BES Grant DE-FG02-91ER14189, NSF Grant CHE 94-04193, and AFOSR Grant F49620-93-1-0067.

REFERENCES

Adelman, D. E., N. E. Shafer, D. A. V. Kliner, and R. N. Zare, 1992, J. Chem. Phys. **97**, 7323.
Aharonov, Y., and B. Bohm, 1959, Phys. Rev. **115**, 485.
Baer, M., 1975, Chem. Phys. Lett. **35**, 112.
Baer, M., and R. Englman, 1992, Mol. Phys. **75**, 293.
Ballhausen, C. J., and A. E. Hansen, 1972, Annu. Rev. Phys. Chem. **23**, 15.
Beärda, R. A., M. C. van Hemert, and E. F. van Dishoeck, 1992, J. Chem. Phys. **97**, 8240.
Bearpark, M. J., M. A. Robb, and H. B. Schlegel, 1994, Chem. Phys. Lett. **223**, 269.
Bernardi, F., S. De, M. Olivucci, and M. A. Robb, 1990, J. Am. Chem. Soc. **112**, 1737.
Bernardi, F., M. Olivucci, I. N. Ragazos, and M. A. Robb, 1992, J. Am. Chem. Soc. **114**, 8211.
Bernardi, F., M. Olivucci, and M. A. Robb, 1990, Acc. Chem. Res. **23**, 405.
Bernardi, F., M. Olivucci, M. A. Robb, and G. J. Tonachini, 1992, J. Am. Chem. Soc. **114**, 5805.
Berry, M. V., 1984, Proc. R. Soc. London, Ser. A **392**, 45.
Berry, M. V., and M. Wilkinson, 1984, Proc. R. Soc. London, Ser. A. **392**, 15.
Bersuker, I. B., 1984a, *The Jahn-Teller Effect and Vibronic Interactions in Modern Chemistry* (Plenum, New York).
Bersuker, I. B., 1984b, *The Jahn-Teller Effect: a bibliographic review* (Plenum, New York).
Bersuker, I. B., and I. Y. Ogurtson, 1986, Adv. Quant. Chem. **18**, 1.
Bishop, D. M., and L. M. Cheung, 1983, J. Chem. Phys. **78**, 1396.
Bishop, D. M., and L. M. Cheung, 1984, J. Chem. Phys. **80**, 4341.
Blais, N. C. and D. G. Truhlar, 1983, J. Chem. Phys. **79**, 1334.
Blais, N. C., D. G. Truhlar, and B. C. Garrett, 1983, J. Chem. Phys. **78**, 2956.
Blais, N. C., M. Zhao, D. G. Truhlar, D. W. Schwenke, and D. J. Kouri, 1990, Chem. Phys. Lett. **166**, 11.
Bohm, A., L. J. Boya, and B. Kendrick, 1991, Phys. Rev. A **43**, 1206.
Bohm, A., B. Kendrick, and M. E. Loewe, 1992, Int. J. Quant. Chem. **41**, 53.
Bohm, A., B. Kendrick, M. E. Loewe, and L. J. Boya, 1992, J. Math. Phys. **33**, 977.

Born, M., and K. Huang, 1954, *Dynamical Theory of Crystal Lattices* (Oxford University Press, Oxford).
Chen, Y. C., D. R. Harding, W. C. Stwalley, and C. R. Vidal, 1986, J. Chem. Phys. **85**, 2436.
Cina, J. A., 1991, Phys. Rev. Lett. **66**, 1146.
Cina, J. A., and V. Romero-Rochin, 1990, J. Chem. Phys. **93**, 3844.
Cina, J. A., T. J. Smith, and V. Romero-Rochín, 1993, Adv. Chem. Phys. **83**, 1.
Crim, F. F., 1993, Annu. Rev. Phys. Chem. **44**, 397.
Delacrétaz, G., E. R. Grant, R. L. Whetten, L. Wöste, and J. W. Zwanziger, 1986, Phys. Rev. Lett. **56**, 2598.
Desouter-Lecomte, M., C. Galloy, J. C. Lorquet, and M. V. Pires, 1979, J. Chem. Phys. **71**, 3661.
Deumens, E., A. Diz, R. Longo, and Y. Öhrn, 1994, Rev. Mod. Phys. **66**, 917.
Eaker, C., 1990, J. Chem. Phys. **93**, 8073.
Englman, R., 1972, *The Jahn-Teller Effect in Molecules and Crystals* (Wiley-Interscience, New York).
Ernst, W. E., and S. Rakowsky, 1995a, Phys. Rev. Lett. **74**, 58.
Ernst, W. E., and S. Rakowsky, 1995b, Ber. Bunsenges. Phys. Chem. **99**, 441.
Fletcher, R., 1981, *Practical Methods of Optimization* (Wiley, New York).
Frey, R. F., and E. R. Davidson, 1990, in *Advances in Molecular Electronic Structure Theory*, edited by T. H. Dunning, Jr. (JAI Press, Greenwich, Connecticut), p. 1.
Gallo, M., and D. R. Yarkony, 1986, J. Chem. Phys. **86**, 4990.
George, T. F., K. Morokuma, and Y.-W. Lin, 1975, Chem. Phys. Lett. **30**, 54.
Gerber, W. H., and E. Schumacher, 1978, J. Chem. Phys. **69**, 1692.
Goldstein, H., 1950, *Classical Mechanics* (Addison-Wesley, Reading, Massachusetts).
Goss-Levi, B., 1993, Phys. Today **46**(3), 17.
Ham, F. S., 1987, Phys. Rev. Lett. **58**, 725.
Hatton, G. J., 1976, Phys. Rev. A **14**, 901.
Hatton, G. J., 1977, Phys. Rev. A **16**, 1347.
Hatton, G. J., W. L. Lichten, and N. Ostrove, 1976, Chem. Phys. Lett. **40**, 437.
Hatton, G. J., W. L. Lichten, and N. Ostrove, 1977, J. Chem. Phys. **67**, 2169.
Herzberg, G., 1966, *Electronic Spectra and Electronic Structure of Polyatomic Molecules* (Van Nostrand Reinhold, New York).
Herzberg, G., and H. C. Longuet-Higgins, 1963, Discuss. Faraday Soc. **35**, 77.
Hettema, H., and D. R. Yarkony, 1994, J. Chem. Phys. **100**, 8991.
Hettema, H., and D. R. Yarkony, 1995, J. Chem. Phys. **102**, 8431.
Hou, Z., and K. D. Bayes, 1993, J. Phys. Chem. **97**, 1896.
Jackiw, R., 1988, Comments At. Mol. Phys. **21**, 71.
Jensen, E., J. S. Keller, G. C. G. Waschewsky, J. E. Stevens, R. L. Graham, K. F. Freed, and L. J. Butler, 1993, J. Chem. Phys. **98**, 2882.
Jensen, J. O., and D. R. Yarkony, 1988, J. Chem. Phys. **89**, 3853.
Johnson, B. R., 1980, J. Chem. Phys. **73**, 5051.
Jungen, C., and A. J. Merer, 1976, in *Modern Spectroscopy: Modern Research*, edited by K. N. Rao (Academic, New York), Vol. II.
Kash, P. W., G. C. G. Waschewsky, R. E. Morss, L. J. Butler, and M. M. Francl, 1994, J. Chem. Phys. **100**, 3463.
Kato, H., and M. Baba, 1995, Chem. Rev. **95**, 2311.
Katriel, J., and E. R. Davidson, 1980, Chem. Phys. Lett. **76**, 259.
Kendrick, B., and C. A. Mead, 1995, J. Chem. Phys. **102**, 4160.
Kendrick, B., and R. T. Pack, 1996a, J. Chem. Phys. **104**, 7475.
Kendrick, B., and R. T. Pack, 1996b, J. Chem. Phys. **104**, 7502.
Kliner, D. A. V., D. E. Adelman, and R. N. Zare, 1991, J. Chem. Phys. **95**, 1648.
Kliner, D. A. V., K.-D. Rinnen, and R. N. Zare, 1990, Chem. Phys. Lett. **166**, 107.
Kojima, T., and T. Nishikawa, 1957, J. Phys. Soc. Jpn. **12**, 680.
Kolos, W., and L. Wolniewicz, 1963, Rev. Mod. Phys. **35**, 473.
Kuntz, P. J., W. N. Whitton, I. Paidarova, and R. Polak, 1994, Can. J. Chem. **72**, 939.
Kuppermann, A., and Y.-S. M. Wu, 1993, Chem. Phys. Lett. **205**, 577.
Lee, T. J., D. J. Fox, H. F. Schaefer, and R. M. Pitzer, 1984, J. Chem. Phys. **81**, 356.
Lengsfield, B. H., and D. R. Yarkony, 1992, in *State-Selected and State to State Ion-Molecule Reaction Dynamics: Part 2 Theory*, edited by M. Baer and C.-Y. Ng (Wiley, New York), p. 82.
Lepetit, B., Z. Peng, and A. Kuppermann, 1990, Chem. Phys. Lett. **166**, 572.
Longuet-Higgins, H. C., 1961, Adv. Spectrosc. **2**, 429.
Longuet-Higgins, H. C., 1975, Proc. R. Soc. London, Ser. A **344**, 147.
Longuet-Higgins, H. C., U. Öpik, M. H. L. Pryce, and R. A. Sack, 1958, Proc. R. Soc. London, Ser. A **244**, 1.
Manaa, M. R., and D. R. Yarkony, 1990, J. Chem. Phys. **93**, 4473.
Manaa, M. R., and D. R. Yarkony, 1992, J. Chem. Phys. **97**, 715.
Manaa, M. R., and D. R. Yarkony, 1993a, J. Phys. Chem. **97**, 4989.
Manaa, M. R., and D. R. Yarkony, 1993b, J. Chem. Phys. **99**, 5251.
Manaa, M. R., and D. R. Yarkony, 1994, J. Am. Chem. Soc. **116**, 11444.
McCarthy, M. I., P. Rosmus, H.-J. Werner, P. Botschwina, and V. Vaida, 1987, J. Chem. Phys. **86**, 6693.
McLachlan, A. D., 1961, Mol. Phys. **4**, 417.
Mead, C. A., 1979, J. Chem. Phys. **70**, 2276.
Mead, C. A., 1980a, Chem. Phys. **49**, 23.
Mead, C. A., 1980b, Chem. Phys. **49**, 33.
Mead, C. A., 1980c, J. Chem. Phys. **72**, 3839.
Mead, C. A., 1983, J. Chem. Phys. **78**, 807.
Mead, C. A., 1992, Rev. Mod. Phys. **64**, 51.
Mead, C. A., and D. G. Truhlar, 1979, J. Chem. Phys. **70**, 2284.
Mead, C. A., and D. G. Truhlar, 1982, J. Chem. Phys. **77**, 6090.
Mead, C. A., and D. G. Truhlar, 1983, J. Chem. Phys. **78**, 6344.
Meiswinkel, R., and H. Köppel, 1990, Chem. Phys. **144**, 117.
Michl, J., and V. Bonacio-Koutecky, 1990, *Electronic Aspects of Organic Photochemistry* (Wiley, New York).
Mielke, S. L., R. S. Friedman, D. G. Truhlar, and D. W. Schwenke, 1992, Chem. Phys. Lett. **188**, 359.
Moody, J., A. Shapere, and F. Wilczek, 1986, Phys. Rev. Lett. **56**, 893.
Morse, M. D., J. B. Hopkins, P. R. R. Langrdige-Smith, and R. E. Smalley, 1983, J. Chem. Phys. **79**, 5316.

Mouflih, B., C. Larrieu, and M. Chaillet, 1988, New. J. Chem. **12**, 65.
Naqvi, K. R., 1972, Chem. Phys. Lett. **15**, 634.
Neuhauser, D., R. S. Judson, D. J. Kouri, D. E. Adelman, N. E. Shafer, D. A. V. Kliner, and R. N. Zare, 1992, Science **257**, 519.
Pacher, T., C. A. Mead, L. S. Cederbaum, and H. Köppel, 1989, J. Chem. Phys. **91**, 7057.
Pople, J. A., 1960, Mol. Phys. **3**, 16.
Renner, R., 1934, Z. Phys. **92**, 172.
Romero-Rochín, V., and J. A. Cina, 1989, J. Chem. Phys. **91**, 6103.
Ruedenberg, K., and G. J. Atchity, 1993, J. Chem. Phys. **99**, 3799.
Scherer, N. F., A. Matro, R. J. Carlson, M. Du, L. D. Ziegler, J. A. Cina, and G. R. Fleming, 1992, J. Chem. Phys. **96**, 4180.
Scherer, N. F., A. J. Ruggiero, M. Du, and G. R. Fleming, 1990, J. Chem. Phys. **93**, 856.
Schiff, L. I., 1960, *Quantum Mechanics* (McGraw-Hill, New York).
Schön, J., and H. Köppel, 1994, Chem. Phys. Lett. **231**, 55.
Schön, J., and H. Köppel, 1995, J. Chem. Phys. **103**, 9292.
Scott, J. L., 1994, ''Vibrational Spectroscopy and photodissociation dynamics of hydroxylamine,'' University of Wisconsin Madison, preprint.
Shapere, A., and F. Wilczek, 1989, Eds. *Geometric Phases in Physics* (World Scientific, Singapore).
Shavitt, I., 1976, in *Modern Theoretical Chemistry*, edited by H. F. Schaefer (Plenum, New York), Vol. 3, p. 189.
Sidis, V., 1992, in *State-Selected and State-to-State Ion-Molecule Reaction Dynamics Part 2. Theory*, edited by M. Baer and C.-Y. Ng (Wiley, New York), Vol. **82**, p. 73.
Smith, F. T., 1969, Phys. Rev. **179**, 111.
Stevens, J. E., H. W. Jang, L. J. Butler, and J. C. Light, 1995, J. Chem. Phys. **102**, 7059.
Stone, A. J., 1976, Proc. R. Soc. London, Ser. A **351**, 141.
Tannor, D. J., R. A. Kosloff, and S. A. Rice, 1986, J. Chem. Phys. **85**, 5805.
Tannor, D. J., and S. A. Rice, 1985, J. Chem. Phys. **83** 5013.
Tannor, D. J., and S. A. Rice, 1988, Adv. Chem. Phys. **70**, 441.
Thompson, T. C., and C. A. Mead, 1985, J. Chem. Phys. **82**, 2408.
Thompson, T. C., D. G. Truhlar, and C. A. Mead, 1985, J. Chem. Phys. **82**, 2392.
Tinkham, M., 1964, *Group Theory and Quantum Mechanics* (McGraw-Hill, New York).
Truhlar, D. G., C. A. Mead, and M. A. Brandt, 1975, Adv. Chem. Phys. **33**, 295.
Truhlar, D. G., J. W. Duff, N. C. Blais, J. C. Tully, and B. C. Garrett, 1982, J. Chem. Phys. **77**, 764.
Tsunekawa, S., 1972, J. Phys. Soc. Jpn. **33**, 167.
Vaghjiani, G. L., 1993, J. Chem. Phys. **99**, 5936.
von Neumann, J., and E. Wigner, 1929, Phys. Z. **30**, 467.
Waschewsky, G. C. G., P. W. Kash, T. L. Myers, D. C. Kitchen, and L. J. Butler, 1994, J. Chem. Soc. Faraday Trans. **90**, 1581.
Werner, H.-J., B. Follmeg, and M. H. Alexander, 1988, J. Chem. Phys. **89**, 3139.
Whetten, R. L., G. S. Ezra, and E. R. Grant, 1985, Annu. Rev. Phys. Chem. **36**, 277.
Wilczek, F., and A. Zee, 1984, Phys. Rev. Lett. **52**, 2111.
Wu, X., R. E. Wyatt, and M. D'Mello, 1994, J. Chem. Phys. **101**, 2953.
Wu, Y.-S. M., and A. Kuppermann, 1993, Chem. Phys. Lett. **201**, 178.
Wu, Y.-S. M., and A. Kuppermann, 1995, Chem. Phys. Lett. **235**, 105.
Xantheas, S., S. T. Elbert, and K. Ruedenberg, 1990, J. Chem. Phys. **93**, 7519.
Yarkony, D. R., 1986, J. Chem. Phys. **84**, 3206.
Yarkony, D. R., 1990, J. Chem. Phys. **92**, 2457.
Yarkony, D. R., 1994, J. Chem. Phys. **100**, 3639.
Yarkony, D. R., 1995, in *Modern Electronic Structure Theory*, edited by D. R. Yarkony (World Scientific, Singapore).
Yarkony, D. R., 1996a, in *Handbook of Atomic Molecular and Optical Physics*, edited by G. L. Drake (AIP, New York), pp. 357–371.
Yarkony, D. R., 1996b, J. Chem. Phys. **104**, 2932.
Yarkony, D. R., 1996c, J. Chem. Phys. **104**, 7866.
Yarkony, D. R., 1996d, J. Phys. Chem., submitted.
Zhang, J. Z. H., and W. H. Miller, 1989, J. Chem. Phys. **91**, 1528.
Zwanziger, J. W., and E. R. Grant, 1987, J. Chem. Phys. **87**, 2954.
Zwanziger, J. W., M. Koenig, and A. Pines, 1990, Annu. Rev. Phys. Chem. **41**, 601.
Zygelman, B., 1987, Phys. Lett. A **125**, 476.